Tunable diode laser absorption spectroscopy for oxygen detection

Lorenzo Cocola
Scuola di Dottorato in Scienze Tecnologie e Misure Spaziali
indirizzo Astronautica e Scienze da Satellite
Supervisore: Prof. G. Naletto
Co-supervisore: Prof. G. Tondello

Contents

Chapter 1

Summary of original contributions

Here is included a short summary of all the original contributions provided in this thesis.

- Driver code for all the WMS based instruments developed at LUXOR. This consists in a piece of code supporting National Instruments data acquisition cards through NI-DAQmx driver for the synchronous synthesis of laser control signals and digitizing of photodetector data.
- Demodulation and filtering code for digital WMS data, for general purpouse application.
- Design, building, testing and evaluation of a prototype instrument for oxygen detection in bottles.
- Design, building, testing and evaluation of two different instrument prototypes for oxygen detection in double glazing window panes.
- Support in designing an instrument for oxygen detection in food packages.
- Building of an experimental setup for GASMAS on apples.
- Experimental campaign with GASMAS on apples exposed to vacuum impregnation.

- Data analysis, processing and discussion for GASMAS with pressure measurement on apples exposed to vacuum impregnation.
- Improvement of an existing design of a GASMAS probe for use on human bodies and scattering food packages.
- Experimental work on GASMAS for human bodies (newborn babies).
- Experimental campaign on GASMAS for scattering food packages.
- Data analysis and discussion on GASMAS for scattering food packages.
- Setup and evaluation of an experimental setup and algorithm for temperature detection through WMS.

Capitolo 2

Riassunto dei contributi originali

Si include un breve riassunto di tutti i contributi originali forniti in questa tesi.

- Codice per il controllo di tutti gli strumenti basati su WMS sviluppati al LUXOR. Questo consiste in un frammento di codice di supporto alle schede di acquisizione dati National Instruments attraverso il driver NI-DAQmx per la sintesi sincrona dei segnali di controllo del laser e per la digitalizzazione dei dati del fotorivelatore.
- Codice per la demodulazione ed il filtraggio di dati digital WMS, di applicazione generale.
- Progettazione, realizzazione, prova e valutazione di un prototipo per il rilevamento di ossigeno in bottiglie.
- Progettazione, realizzazione, prova e valutazione di due diversi prototipi di strumenti per il rilevamento di ossigeno in pannelli di vetrocamera.
- Supporto alla progettazione di uno strumento per il rilevamento di ossigeno in contenitori alimentari.
- Costruzione di un setup sperimentale per la GASMAS su mele.
- Campagna sperimentale con GASMAS su mele esposte a vacuum impregnation.

- Analisi dei dati, elaborazione e discussione della GASMAS con misura di pressione su mele esposte a vacuum impregnation.
- Miglioramento di un progetto esistente di sonda GASMAS per l'uso su corpo umano e contenitori alimentari diffondenti.
- Sperimentazione con GASMAS su corpi umani (neonati).
- Campagna sperimentale su GASMAS per contenitori alimentari diffondenti.
- Analisi di dati e discussione su GASMAS per contenitori alimentari diffondenti.
- Messa a punto e valutazione di un dispositivo sperimentale e di un algoritmo per la misura di temperatura tramite WMS.

Chapter 3

Abstract

The evolution of diode laser sources for optical communications during the last years led to commercial availability of devices which are suitable for gas absorption spectroscopy in the near and mid infrared. In this work it is shown how the traditional limits of Tunable Diode Laser Absorption Spectroscopy are addressed with digital signal processing techniques and careful optical design towards the realization of gas sensing instruments with the stability, robustness and reliability that are required in an industrial environment. Being one of the most challenging gases to be sensed with this technique, oxygen was considered under many measurement aspects such as:

- Non invasive monitoring;
- Gas in scattering media sensing;
- Sensing with back-scattering targets;
- Pressure measurement techniques for weak absorption signals;
- Time resolved, dynamic sensing;
- Temperature measurement through absorption spectroscopy.

Many of these aspects were considered together, leading to the developement of instruments tailored for real life industrial applications such as:

- Oxygen sensing in partially transparent containers such as wine or soft drink bottles;

- Monitoring of double glazing insulating glass gas filling machines;
- Oxygen sensing in containers with backscattering targets such as food packagings.

Other applications for the technique and experiments involving Gas in Scattering Media Absorption Spectroscopy were explored during a 6 months period at the Lunds Universitet - Lunds Tekniska Högskola - Atomfysik (Sweden) under the supervision of Prof. S. Svanberg:

- Gas probing into porous fruit samples;
- Gas sensing inside the human body as a medical diagnosis technique;
- Oxygen measurement in fully scattering food containers;
- Multi-line absorption spectroscopy as a temperature measurement.

Capitolo 4

Sommario

L'evoluzione delle sorgenti laser a diodo per le comunicazioni ottiche negli ultimi anni ha portato ad una disponibilità commerciale di dispositivi che si prestano alla spettroscopia di assorbimento di gas nel vicino e medio infrarosso. In questo lavoro si mostra come i limiti tradizionali della spettroscopia di assorbimento a diodi laser sintonizzabili vengano affrontati con tecniche di elaborazione numerica di segnali ed una attenta progettazione ottica rivolta alla realizzazione di strumenti per il rilevamento di gas caratterizzati dalla stabilità, robustezza ed affidabilità necessari per un ambiente industriale. Trattandosi di uno dei gas più critici per il rilevamento con questa tecnica, l'ossigeno è stato affrontato sotto molteplici aspetti di misura come:

- Monitoraggio non invasivo;
- Rilevazione di gas in mezzi diffondenti;
- Rilevazione tramite bersagli retrodiffondenti;
- Tecniche di misura di pressione per deboli segnali di assorbimento;
- Rilevazione dinamica con risoluzione temporale;
- Misure di temperatura attraverso spettroscopia di assorbimento.

Molti di questi aspetti sono stati considerati simultaneamente portando allo sviluppo di strumenti appropriati ad un uso nel mondo reale in applicazioni industriali quali:

- Rilevazione di ossigeno in contenitori parzialmente trasparenti come bottiglie di vino e bibite;
- Controllo di macchine per il riempimento di pannelli isolanti in vetrocamera;
- Rilevazione di ossigeno in contenitori con bersagli retrodiffondenti, quali confezioni alimentari.

Altre applicazioni della tecnica ed esperimenti sulla spettroscopia di assorbimento di gas in mezzi porosi sono stati esplorati durante un periodo di 6 mesi presso Lunds Universitet - Lunds Tekniska Högskola - Atomfysik (Svezia) sotto la supervisione del Prof. S. Svanberg:

- Analisi di gas in campioni porosi di frutta;
- Rilevazione di gas all'interno del corpo umano come tecnica per la diagnostica medica;
- Misura di ossigeno in contenitori completamente diffondenti per alimenti;
- Spettroscopia di assorbimento multi-riga come misura di temperatura.

Chapter 5

Introduction

5.1 Absorption spectroscopy

Absorption spectroscopy is a generic term to describe every measurement technique based on the phenomenon of absorption of radiation as a function of wavelength caused by interaction with the sample. The intensity of this absorption varies with wavelength because energy transitions between radiation and matter can more likely happen between two well defined quantum mechanical states of the sample. This model yields to a structure of different absorption lines (spectrum) which is a fingerprint of the material. The frequency of the lines depends on the electronic, molecular and crystal structure of the sample as well as environmental factors such as pressure, temperature and electromagnetic fields. Going further in analysis of single absorption lines, the shape and width are essentially determined by the environment.
Various frequency ranges of radiation correspond to different types of transitions:

Spectral region	Physical process
γ rays	Nuclear transitions
X rays	Inner electron transitions
UV - Visible	Outer electron transitions
Visible - IR	Molecular vibrations
IR - microwaves	Molecular rotations
Microwaves - radio	Spin orientations

IR radiation is related to changes of rotovibrational states of the material molecules, so IR spectroscopy can be used to make non-invasive analysis, so it is particularly suited for gas detection. Traditionally, absorption spectroscopy was accomplished with wide-band radiation sources and monochromators or interferometers leading to expensive and complex measurement setups. The availability of narrow band, tunable sources of radiation made a major improvement for the realization of simple, robust and reliable spectroscopic instruments, especially in the field of gas detection where the entire required tuning range can be very narrow. This thesis is mostly about gaseous oxygen detection on $760nm$ band, which is the strongest available in the IR region and can be investigated with commercially available single mode tunable laser diodes. Moreover, in this region there is almost no interference between oxygen absorption and the one of other abundant species.

5.1.1 Lambert-Beer law

For a sample of absorbing matter, the ratio between transmitted (I) and incident (I_0) radiation intensity at wavelength λ after a path of known length l is called transmittance and is given by:

$$T = \frac{I}{I_0} = e^{-\sigma_\lambda l N} \tag{5.1}$$

where σ_λ is the cross-section for the absorption transition at wavelength λ and N is the density of the absorpting particles, expressed as a number of particles per volume unit. Another parameter often found is absorbance $A = -\log \frac{I}{I_0}$.

5.1.2 Absorption profiles

A further, high resolution analysis of spectral absorption lines can reveal their shape and width, which are dependent on sample conditions.

The lower limit of linewidth is due to the finite duration of the radiative process. As stated by Fourier transform theory, a purely sinusoidal wave has infinite duration and this is not possible in nature. So ΔE, the energy uncertainty (which is related to frequency by Planck's law), is bound to the average life Δt of the energy level by Heisemberg's uncertainty principle:

$$\Delta E \Delta t \geq \hbar \tag{5.2}$$

From the laws of quantum mechanics and harmonic oscillator follows the analytical expression of an absorption profile with an average emission duration equal to $1/\gamma$:

$$\tau(\nu) = \frac{\gamma}{\gamma^2 + (\nu - \nu_0)^2} \tag{5.3}$$

This is a lorentzian bell-shaped function centered around ν_0 with an HWHM equal to γ. It should be noted that every absorpting particle in the system is subject to this kind of broadening.

Collision broadening

A possible cause for further broadening of spectral lines is due to collision between particles. When a collision happens during a transition process, the interaction between particles causes a shift in energetic levels and so an alteration in the corresponding frequency.
The following approximations are needed to obtain a simple model of collision broadening:

- Elastic collisions, without energy losses between kinetic and excitation energy;
- Short duration of collision process, compared to average life without collisions;
- Emission and absorption during the collision process are negligible.

Under these approximations the collision can be thought as an instantaneous loss of coherence in the wave. This leads to the same lorentzian absorption profile shape, where γ is now the inverse of the average life without collisions.
RMS speed and mean free path values obtained from the kinetic theory of gases leads to the following expression for collision broadening:

$$\delta_u{}^{\nu} = \frac{4N\rho^2 p}{\sqrt{RT\mu\pi}} \tag{5.4}$$

with cross section ρ^2 (defined as the square of the minimum distance between particles for no influence on energy levels), Avogadro constant N, pressure p, gas constant R, particle mass μ and temperature T.

Doppler broadening

The fact that particles in a system are in motion leads to a different frequency shift for each single particle. This is due to Doppler effect and depends on the relative velocity component in the direction between source and receiver. The resulting frequency shift δ_ν is such as

$$\frac{\delta_\nu}{\nu_0} = \frac{u}{c} \tag{5.5}$$

where u is the velocity component along the observation direction and c is the speed of light. Using the Maxwell distribution for the velocity of particles along one direction the FWHM for the only Doppler broadening can be expressed as:

$$\delta_d{}^\nu = \frac{2\nu_0}{c}\sqrt{\frac{2RT\ln 2}{\mu}} \tag{5.6}$$

Considering only the Doppler broadening component leads to a gaussian line profile.

Combination of different broadening sources

When more than one broadening effect is present, the resulting shape is determined by the convolution of all the single contribution shapes. In the very common case of simultaneous collision and Doppler broadening, the resulting shape is the convolution of a lorentzian and a gaussian function. This shape is known as a Voigt profile. A comparison between lorentzian, gaussian and Voigt profiles are shown in figure 5.1. For the same HWHM, the gaussian shape has a higher peak intensity.

For absorption lines in a gas at STP, it is typical to obtain shapes dominated by collision broadening and so, lorentzian profiles. As an example [5], pressure broadening at room temperature for the oxygen lines in the A band ($760nm$ or $13122cm^{-1}$) accounts for a broadening which varies in a range between 0.038 to $0.063cm^{-1}/atm$. The difference between self and N_2 broadening is not significant. At room temperature and ambient pressure, the measured linewidth is around $3GHz$ with a line profile that is largely lorentzian.

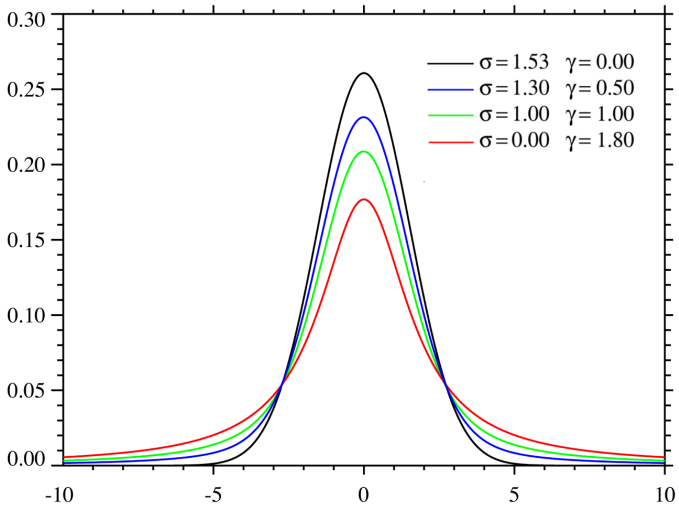

Figure 5.1: Example of different Voigt profiles with identical FWHM, ranging from fully Gaussian ($\gamma = 0$) to fully Lorentzian ($\sigma = 0$).

5.2 TDLAS technique

TDLAS stands for *Tunable Diode Laser Absorption Spectroscopy* and refers to the technique of using a laser diode as a monochromatic source which can be scanned across the absorption feature of interest.
In a laser diode, the optical gain wavelength range of the active medium is often wide enough to have a useful tuning range. To achieve single mode laser operation with a narrow emission linewidth, some kind of optical resonator has to be used. This is generally accomplished by:

- using an external optical cavity, which can be made tunable by external means (ECL devices, figure 5.2);
- etching a periodic optical structure along the active medium (DFB lasers, figure 5.3);
- making the same active medium shaped to achieve single mode operation (VCSEL devices, figure 5.4).

While the first method requires external optical devices which may be delicate and expensive, the latter two cases (VCSELs and DFB lasers) do not rely

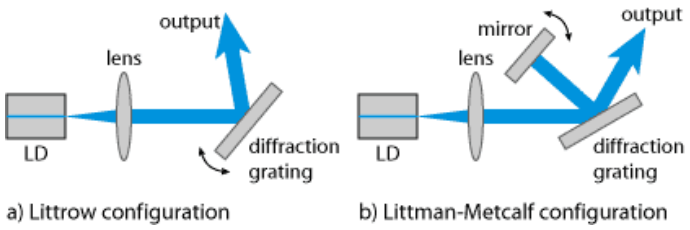

Figure 5.2: Tunable external-cavity diode lasers in Littrow and Littman-Metcalf configuration.

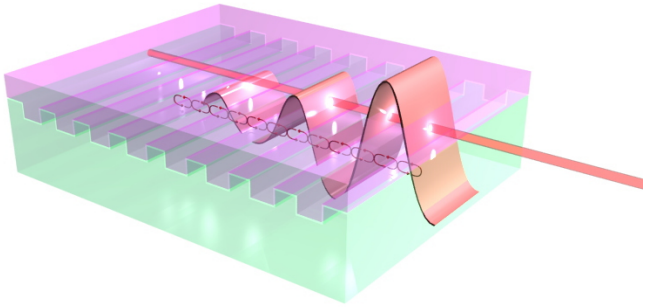

Figure 5.3: Operation principle of a distributed feed-back diode laser.

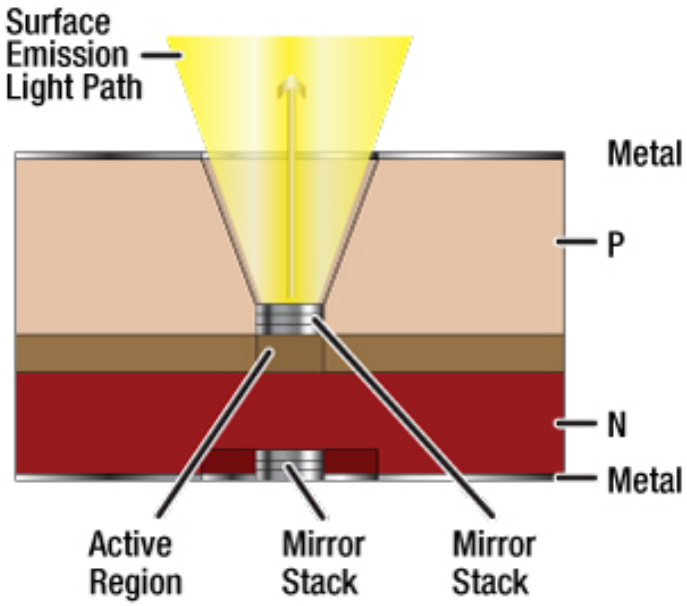

Figure 5.4: Schematic of a vertical cavity surface emission laser.

on external component except for a mean of thermally controlling the active medium and can achieve side mode suppression ratios above $30dB$. However, in this case, tuning is not as straightforward. There are essentially two ways to tune those lasers:

- varying the temperature of the laser;
- varying the injection current.

These methods work because of slight variations of the cavity optical length induced by thermal expansion or refractive index variation and compared to external cavity tuning they are very fast: thermal tuning speed is limited by the thermal inertia of the device while injection current tuning speed is even faster. As it will be described in the next section, speed can be important in some absorption spectroscopy techniques. The negative effects of those tuning methods (especially injection current tuning) are wide emitted power fluctuations. This kind of lasers are usually available with power ratings from $10\mu W$ (VCSEL) to $50mW$ (DFB) and emission linewidth range from $100MHz$ to $2MHz$.

5.3 Direct-absorption spectroscopy

Direct-absorption spectroscopy (figure 5.5) is useful to investigate strong absorption features. It is usually suitable to address strong lines in the mid-IR, such as the carbon dioxide ones near $2\mu m$ shown in figure 5.6. The principle is the same of traditional absorption spectroscopy: a linear sweeping of the source wavelength and the acquisition of the signal emerging from the sample. The measurements can be obtained by fitting the acquired signal with a proper model, and interpretation of the resulting line parameters (intensity and width) is straightforward.

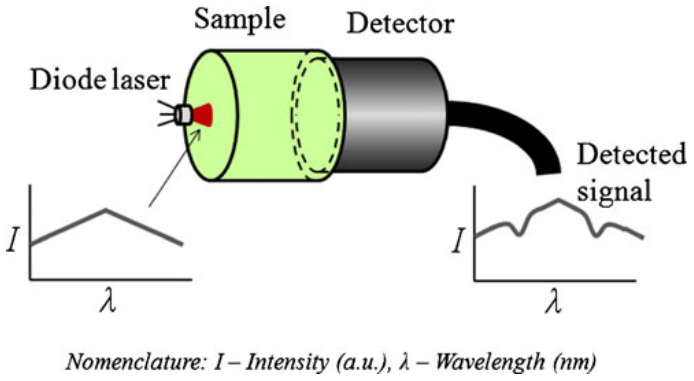

Figure 5.5: Optical setup for direct absorption spectroscopy.

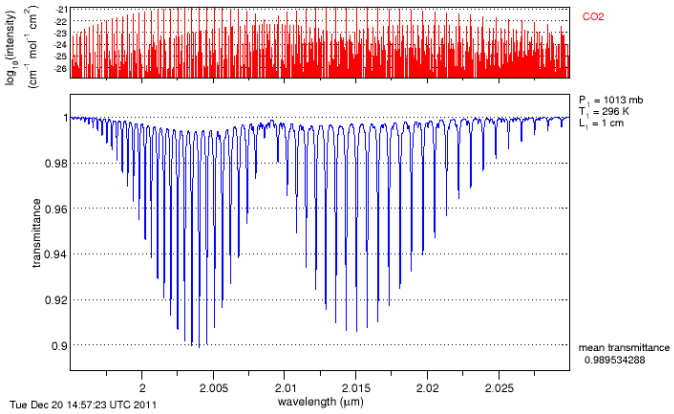

Figure 5.6: Example of the strong absorption features in the $2\mu m$ band for STP pure carbon dioxide, 1cm path length. The high intensity of those lines allows direct absorption spectroscopy on this band for most applications.

5.4 WMS

WMS (Wavelength Modulation Spectroscopy) is a technique used to overcome the traditional problems of Direct-absorption spectroscopy when investigating low absorbances, where there is a need to resolve a tiny absorption feature over an intense source signal. This method works by applying a small, sinusoidal wavelength modulation over the linear scanning of the source at a much higher frequency. This leads to instantaneous frequency and amplitude of emitted signal:

$$\nu(t) = \bar{\nu} + \Delta\nu \cos \omega_m t \tag{5.7}$$

$$I_0(t) = \bar{I_0} + i_0 \cos(\omega_m t + \psi) \tag{5.8}$$

where the scanning frequency is low compared to ω_m. The signal received by the photodetector is:

$$I(t) = I_0(t)\tau(\nu(t)) \tag{5.9}$$

where $\tau(\nu(t))$ is the absorption profile. Using eq. 5.7 as $\nu(t)$ and expanding in Fourier series results in

$$\tau(\nu(t)) = \sum_{k=0}^{k=+\infty} H_k(\bar{\nu}, \Delta\nu) \cos(k\omega_m t) \tag{5.10}$$

where $H_k(\bar{\nu})$ can be expressed as

$$H_0(\bar{\nu}, \Delta\nu) = \frac{1}{2\pi} \int_{-\pi}^{+\pi} \tau(\bar{\nu} + \Delta\nu \cos u) du \tag{5.11}$$

$$H_k(\bar{\nu}, \Delta\nu) = \frac{1}{\pi} \int_{-\pi}^{+\pi} \tau(\bar{\nu} + \Delta\nu \cos u) \cos ku du, \ k > 0 \tag{5.12}$$

The analytical expression for those terms could not be given, but for small absorbance values and small modulation depths (compared to spectral absorption linewidth) the demodulated terms H_k are a good approximation of the k^{th} derivative of the absorption profile.

Given an ideal photoreceiver bandwidth, for the 1^{st} and 2^{nd} harmonics the demodulated signal can be written as

$$S_1(\bar{\nu}) = \frac{i_0}{2} H_2(\bar{\nu}, \Delta\nu) \cos(2\psi + \phi) + \bar{I}_0 H_1(\bar{\nu}, \Delta\nu) \cos(\psi + \phi) + i_0 H_0(\bar{\nu}, \Delta\nu) \cos\phi \tag{5.13}$$

$$S_2(\bar{\nu}) = \frac{i_0}{2} H_3(\bar{\nu}, \Delta\nu) \cos(2\psi + \phi) + \bar{I}_0 H_2(\bar{\nu}, \Delta\nu) \cos(\psi + \phi) + i_0 H_1(\bar{\nu}, \Delta\nu) \cos\phi \tag{5.14}$$

Usually the main contributions are respectively H_1 and H_2 because amplitude modulation i_0 is small compared to I_0. An example of the resulting signal shapes is shown in figure 5.7D. The relationship between linewidth (figure 5.7C) and demodulated signal shape depends on the modulation depth.

5.4.1 Practical implementations of the signal processing stage

The signal can be demodulated with homodyne technique and be processed to extract information about the sample. The typical demodulation system is made of:

- a properly shaped bandpass filter, centered around $k\omega_m$ to select the desired harmonic k^{th} and to cut out unwanted photoreceiver noise;
- a baseband shift (frequency mixer) to obtain a baseband signal to be further processed;

In the real word, such a processing chain can be implemented in several different ways:

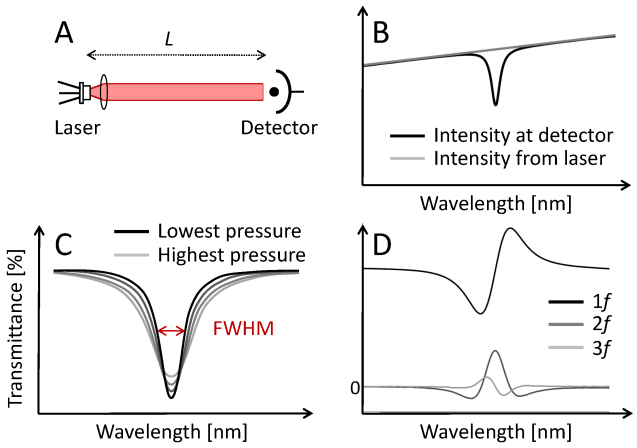

Figure 5.7: (A) Optical channel. (B) Direct absorption signal. (C) Effects of line broadening. (D) 1st, 2nd and 3rd component of a Wavelenght Modulation Spectroscopy signal, baseband shifted.

- passive approach, with filter and mixing stage accomplished by passive RF devices, suitable for higher frequency operating ranges (figure 5.8);
- active electronic approach (lock-in type), using analog devices such as op-amp active filters and translinear active multipliers (figure 5.9);
- software-defined digital approach, where the photodetector signal is simply acquired by an A/D converter and a digital device takes care of all the processing (figure 5.10).

The latter technique has a significant advantage when thinking to a possible measurement device suitable for use in a space or industrial environement: the A/D section can be synchronous with laser modulation circuitry, requiring no external triggering methods or lock-in frequency reference channels. The result is a simple, self-consistent device able to obtain very high signal-to-noise and signal-to-interference ratios even in harsh environements by averaging multiple spectral scans with virtually no jitter. Filters and baseband conversion can be easily done respectively by multiplication and shifting in the FFT domain without adding any noise to the signal, while signal averaging leads to an arbitarily narrow (with increasing integration time) comb filtering at multiples

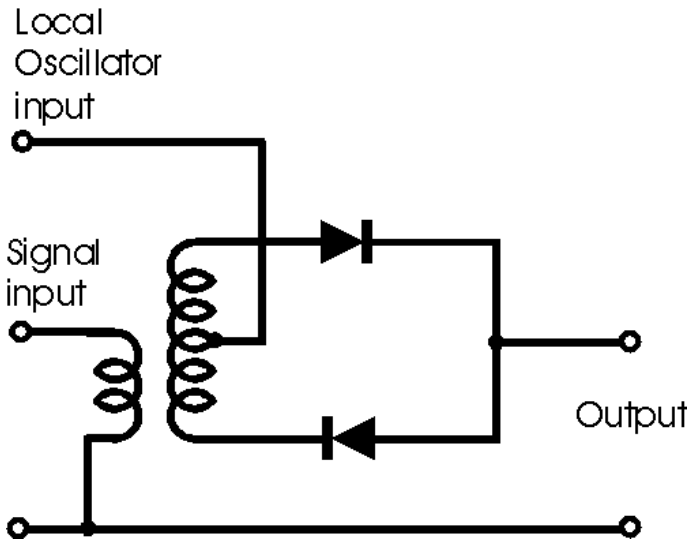

Figure 5.8: A diode based single-balanced RF mixer.

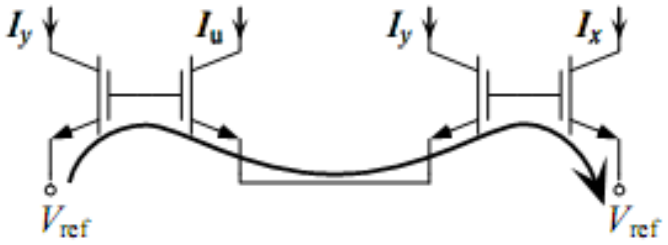

Figure 5.9: A translinear loop. The exponential relation between voltages and currents in the translinear elements is used to transform voltage sums (Kirchhoff voltage law) into current products, thus performing analog multiplications in hardware.

of the scanning frequency. Furthermore, given a high enough sampling rate at the A/D conversion stage, data from multiple harmonic channels are acquired simultaneously.

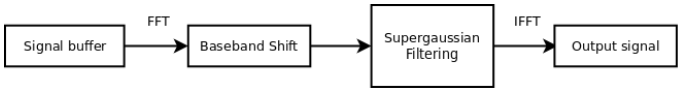

Figure 5.10: dWMS demodulation block diagram.

5.5 Oxygen absorption features in the 760nm band

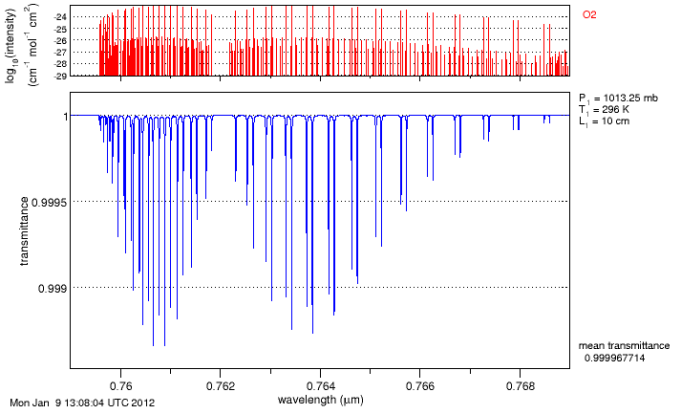

Figure 5.11: Simulated absorption spectrum of a 5cm STP air path. Sensing on those lines usually requires more sophisticated techniques rather than direct absorption spectroscopy.

For the TDLAS method applied to oxygen, the only available choice of absorption lines accessible through current laser diode technology are located in two bands around 760 and 763nm, both with maximum peak absorbance in the 10^{-24} cm/mol (HITRAN absorbance units). As a comparison, this gives a transmittance ratio of 0.999 for a 5cm optical path in ambient air, as shown by the simulated spectrum in figure 5.11. For most oxygen metering applications, this figure sets the ultimate sensitivity limit.

Pressure broadening leads to complete line overlapping at pressures greater than 10 bar, to the point that lines in the 760 nm band are no more discernible over 20 bar.

An interesting feature of the 760 nm band is the availability of 10 lines in a 1 nm range. This can be useful for single source multi-line TDLAS, enabling temperature measurement.

5.6 Error sources in WMS measurements

5.6.1 Noise

Electrical and optical sources of noise can often be a limiting factor in a WMS experiment. Due to the limited power of the available laser sources, experiments involving scattering samples or samples contained in a dark media can easily reduce available light on the detector to critical level. An optimization of the detector type (photodiode, avalanche photodiode, photomultiplier tube) and detector size can be relevant for the application.

Another noise issue to be considered is the extremely low current signal required for the wavelenght modulation of VCSEL diodes. Proper low noise board layout and design are mandatory when working with these sources.

The choice of lock-in modulation frequency in a WMS experiment is given by noise corner considerations: noise in the system can be dominated by the 1/f term under the noise corner, while being white at higher frequencies. For a typical WMS setup it is thus optimal to operate at frequencies above the kHz range, accordingly with bandwith requirements of the modulation and detector stage.

5.6.2 Interference

A WMS measurement setup operating near its detection limit has to work with very low absorbance (around 10^{-6}) and so has to deal with very low fluctuations of the optical path transmissivity. While the single optical components in the system can have a reasonably flat transmission coefficient as a function of wavelength in the source scanning range, the transmission coefficient of a whole optical system containing windows, lenses, sample vessel and other surfaces often shows periodic fluctuations due to interference effects. The resulting signal

is affected by slowly drifting interference artifacts, which in a WMS signal can appear as shown in figure 5.12. An accurate optical design can often mitigate those effects, but some applications can include optical elements in the sample which are not part of the instrument and so are out of designer's control.

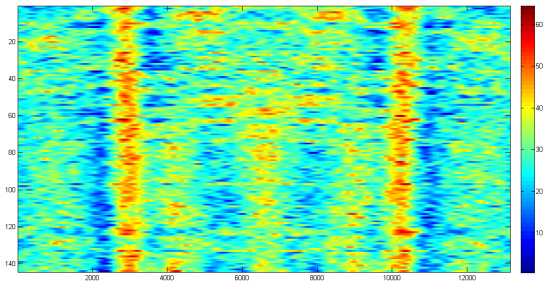

Figure 5.12: Example representing fluctuations of interference pattern due to thermal drifts during time (vertical axis). Demodulated 2ω signal is represented in false colours where each horizontal line represents a measurement. The two strong, darker, bordered lines represent absorption signal, while other vertical symmetrical line-like shapes are due to fluctuating interference effects.

Etalon effects

Any transparent medium with two reflective surfaces forms a Fabry-Pérot interferometer. Its transmission spectrum presents periodic fluctuations due to interference between multiple reflections of light into the medium.

Considering the propagation of a ray with incidence angle equal to θ, the phase difference between two succeding reflections is

$$\delta = \frac{2\pi}{\lambda} 2nl\cos\theta \tag{5.15}$$

where l is the distance between reflective surfaces, n is the refractive index of the medium and λ is the wavelength. Said R the reflectance of the surfaces, the transmittance function can be written as:

$$T_e = \frac{1}{1 + F\sin^2(\delta/2)} \tag{5.16}$$

where $F = \frac{4R}{(1-R)^2}$ is called finesse.

The period of transmittance fluctuations is called the free spectral range and is equal to:

$$\Delta\lambda = \frac{\lambda_0^2}{2nl\cos\theta + \lambda_0} \tag{5.17}$$

When the finesse is low, as in the case of etalons formed by stray reflections, the transmission fluctuation as a function of wavelength is approximated by a sinusoid. The phase of this artifact is random, unpredictable and is usually affected by thermal drifts, as the optical parts and mounts used do not have an interferometric-scale stability.

It is important to remember that real experiments are usually affected by the superimposition of cavity effects from different reflecting components; in this case the transmittance recorded at the receiver end has no more a single sinusoidal shape but shows a sum of many different frequencies. The nature of the etalon pattern depends upon the complexity of the optical setup and can vary from the very simple case of pure sinusoidal, such that it is possible to use a notch filter to mitigate the effects, to the case of GASMAS where interference from multiple scattering centers in the sample media generates a noise-like signal.

Self mixing

When an active medium such as a laser diode has some of its emission reflected back in the cavity as in figure 5.13, an etalon is formed. In this case, small wavelength dependent fluctuations can induce strong power variations in the output by varying the balance of the active cavity. This phenomenon can be very easily observed in lasers with low output mirror reflectivity such as DFBs where any back-reflected power is coupled into the active cavity. Increasing returned intensity, the following effects can be osserved:

- strong fluctuations in power output;
- increased power output;
- increased emission bandwidth;
- loss of single-mode operation;
- loss of coherence or permanent damage of the cavity, with catastrophic optical damage.

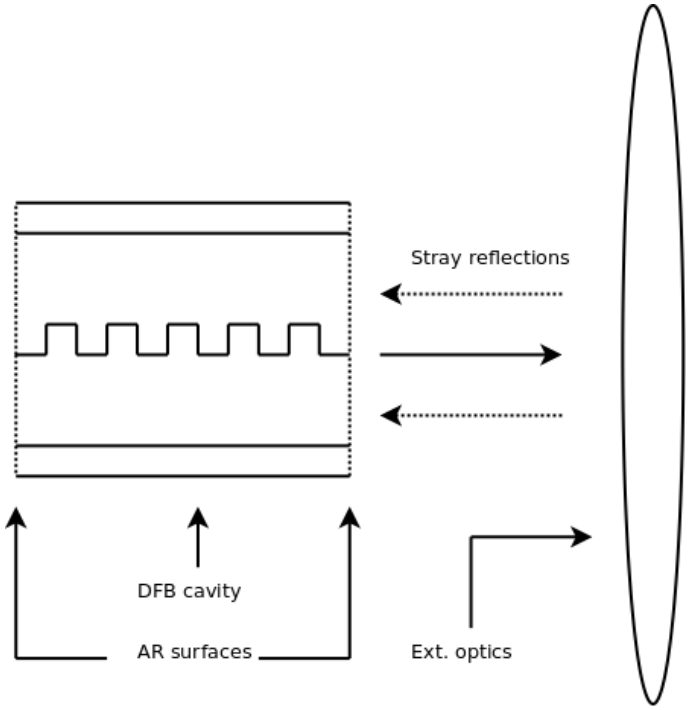

Figure 5.13: Self mixing phenomenon.

Even if kept below levels that can affect large-signal behaviour of the source, self mixing will introduce wavelength dependent artifacts very similar to the ones observed in passive optics affected by etalon effects.

5.6.3 Remedies against interference effects

In a sensitive TDLAS measurement it could be very important to suppress fluctuations originating from interferometric phenomena. While they should be reduced as much as possible by careful optical design, AR coatings, index-matching, tilting and/or wedging optical elements to avoid spatially overlapping stray reflected spots, in some cases even the residual interference can be an issue.

Common methods to take care of this problem are based on dithering the optical length of unwanted cavities to average out the interference signal during time. The required variation of optical cavity length is of the same order of wavelength: for example a mechanical vibration applied to an optical element can be enough to average out the interference signal.

The main drawback of this strategy is that the vibration and the time-variable interference effect are still noises requiring time to be averaged out by integration.

The implementation of dithering methods is a matter that requires a specific tailoring for each application depending to optical configuration, mass of the sample and optical parts, eventual scattering properties of involved elements and requirements on allowable integration time.

Chapter 6

Applications

Gas detection is a very wide field where an enormous range of application-specific different techniques can be found. While many methods require physical contact between the sample and the instrument, one of the main interesting points in absorption spectroscopy is that only optical interaction with the sample is required. This is particularly useful because:

- degradation of the instrument by the sample/environment and vice-versa can be avoided;
- the sample may be located far from the instrument and measurement information can be carried by the propagation of an optical signal.
- the interaction length with the sample may vary, so sensing may be distributed over a long distance or relatively localized.

Such features make this method in fields like:

- non-invasive measurement, as inside packaging gas monitoring;
- quality control in modified atmosphere packaging;
- repetitive measurement for industrial process control;
- remote atmosphere sensing for environmental monitoring;
- gas leak detection by airplane flight over pipelines;

- biomedical measurements on human breath and gas included into sinuses [3];

Amongst the instruments that will be discussed in this work, we focused on

- measurement inside closed bottles, for industrial bottling process monitoring, corking machine quality control, oenology and wine aging;
- measurement on double-glazing insulating glass panels production lines, for automation and quality control of inert gas filling machinery;
- measurement into food packages, for controlled atmosphere food preservation.

6.1 Space applications of TDLAS

There are many application of TDLAS in space, for both research, ground based application and flight measurements.

6.1.1 Combustion diagnosis

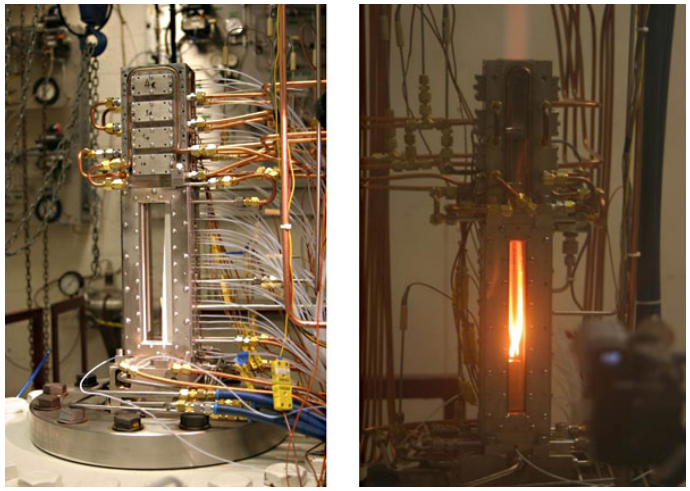

Figure 6.1: Example of supersonic combustion facility with optical access for diagnosis (courtesy of University of Virginia).

Analysis of the species found in a combustion process as well as in exhaust gases is made possible with TDLAS. Among the interesting ones commonly monitored in combustion byproducts are:

- Residual oxygen;
- Carbon dioxide;
- Carbon monoxide;
- Nitrogen oxides;
- Residual fuels;

While many electrochemical detectors are already available, inexpensive and widely used in both industrial and consumer market, such as zirconia oxygen sensors (lambda sonds) or electrochemical gas meters used in furnaces or leak detectors, TDLAS based detection offers many advantages on this field:

- Insensitivity to temperature (or even simultaneous temperature detection)
- Tolerance to harsh environments of combustion due to non-invasiveness
- Stability with time, not being affected by poisoning.

6.1.2 Gas detection instruments on space missions

Experiments for the TDLAS detection of methane and its isotopes for in situ measurements on the surface of Mars have been reported [2]. Moreover, the recent availability of QC (Quantum Cascade) lasers and detectors further extended the spectral region which can be addressed with TDLAS towards mid IR. This region is very interesting for trace-gas detection, due to the presence of many strong absorption lines.

6.1.3 Satellite, balloon and aircraft based gas detection

Between terrestrial and space application of TDLAS there are long-path and LIDAR techniques for monitoring of atmospheric polluttants, such as DOAS (differential optical absorption spectroscopy) and DIAL (differential absorption LIDAR). Examples are reported in figure 6.4 and 6.2

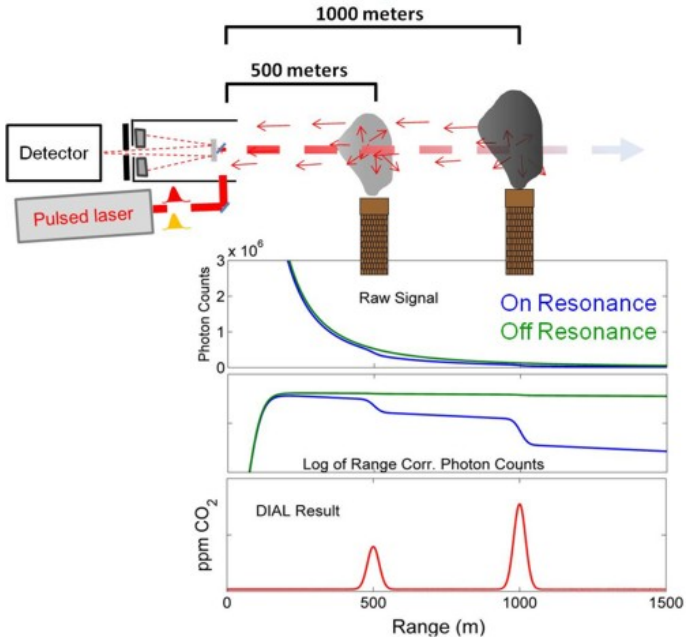

Figure 6.2: DIAL (LIDAR) operation schematics for environmental monitoring (courtesy of NIST).

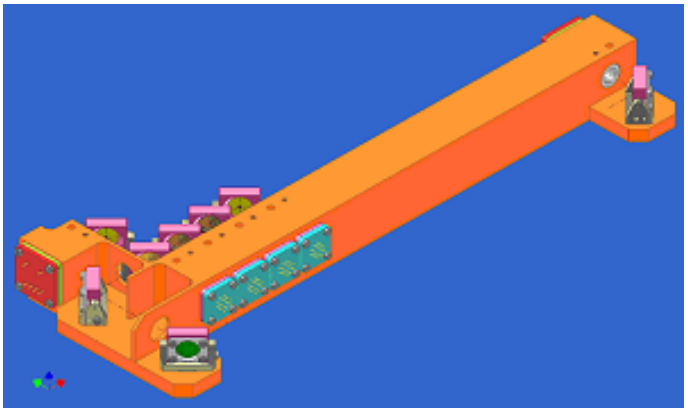

Figure 6.3: PHOBOS-GRUNT: GAP TDLAS 4 channel TDLAS spectrometer package for water, carbon dioxide, acetylene with isotope sensitivity for use on Phobos (courtesy CNES).

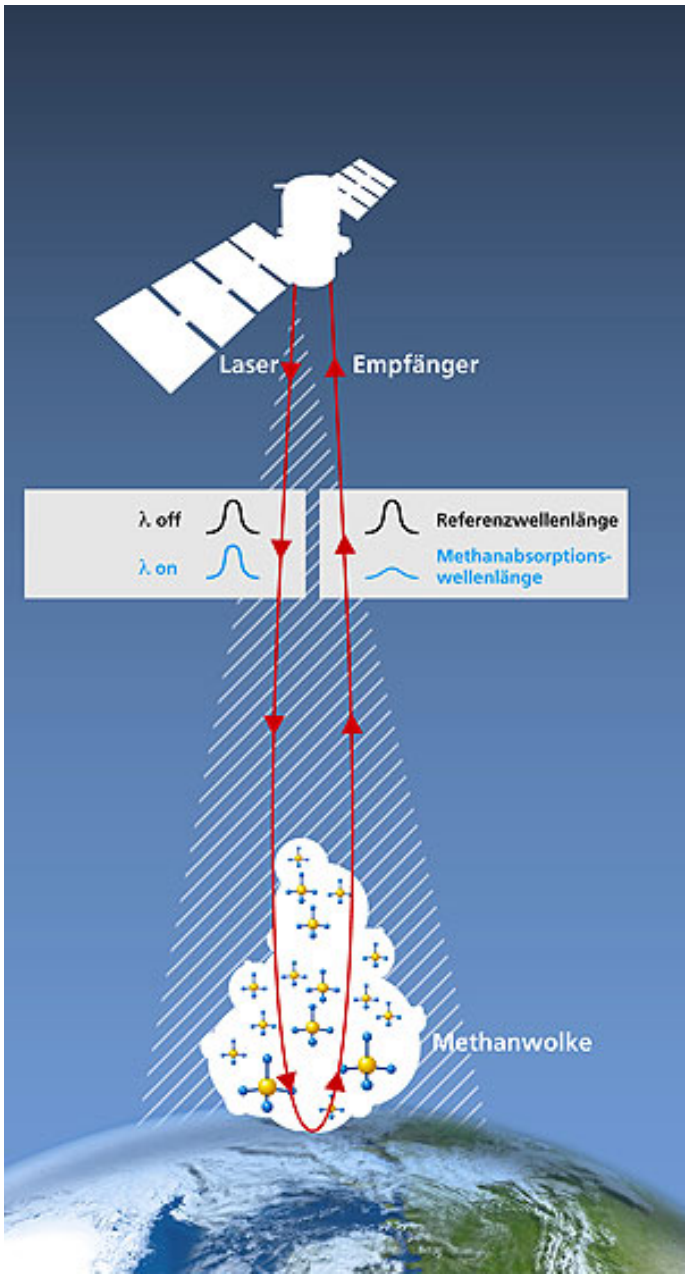

Figure 6.4: Methane sensing LIDAR satellite (courtesy German Aerospace Center).

The traditional LIDAR principle, where backscattering of a light pulse propagating in the environment is evaluated as a function of delay time to resolve scatterer's distance, can be applied at different "on" and "off" wavelengths (or multiple wavelenghts) to add sensitivity about the nature of the scatterer.

Chapter 7

WMS instrument overview

Various applications of WMS-TDLAS have been considered and will be discussed in this work. They are mostly about oxygen detection but it is important to note that the digital signal processing approach is common to all experiments and may be shared by other gas sensing applications as well.

7.1 Digital WMS setup summary

In this section it will be presented a setup to implement industrial measurement applications based on WMS-TDLAS.

7.1.1 Source and modulation stage

Various laser diodes have been used for oxygen detection, of both VCSEL and DFB type.

- ULM Photonics Single Mode VCSEL, 763nm with integrated TEC and feedback thermistor, 250μW typical power output (figure 7.1);
- Avalon Photonics Single Mode VCSEL, 763nm with integrated TEC and feedback thermistor, 300μW typical power output;
- Eagleyard Photonics Single Mode DFB laser, 760nm, with integrated TEC and feedback thermistor, 40mW typical power output. Those sources are available both in pigtailed and open versions (figure 7.2 and 7.3);

Figure 7.1: Typical VCSEL lasers in different casings. The larger ones are provided with built in TEC element and temperature sensing thermistor.

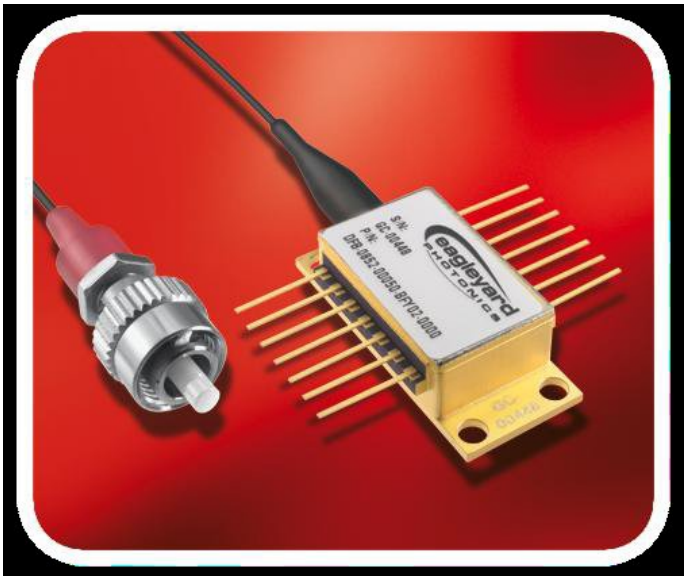

Figure 7.2: A fiber pigtailed DFB laser. The butterfly casing is very common in the telecommunications environment, usually provided with built in TEC element, temperature sensing thermistor and reference photodiode.

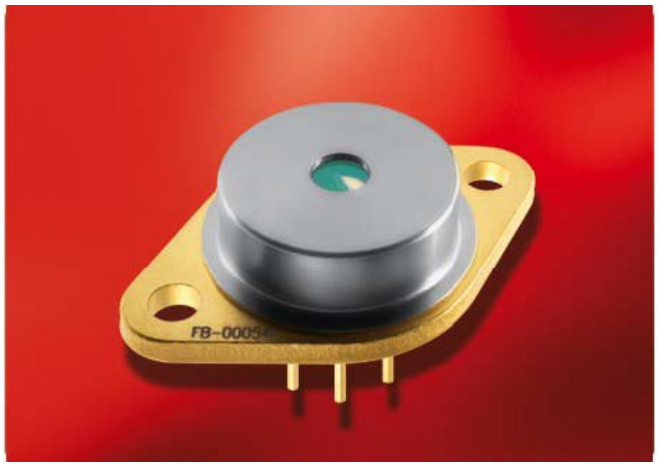

Figure 7.3: A high power (over 50mW) DFB laser. The heavy TO3 casing (originally developed for power transistors) provides all the features needed for thermal and power control, as well as a good thermal interface for heatsinks.

The VCSEL sources have been run by a Thorlabs VITC002 board (figure 7.4), which is an OEM device to provide both an externally-controlled laser diode current source and a closed loop temperature control matched for the TEC cell and thermistor used in common laser diode packaging.

The DFB lasers is driven by two laboratory devices, LDC200 and TED200, respectively for current and temperature control.

All these devices are provided with safety features such as interlocks, soft start, shorting relays for ESD protection and programmable current limiting. Laser diodes are very sensitive devices and operation with those features is mandatory.

The external current control gives full control of laser diode current with a -3dB bandwidth of 100kHz. For modulation above this frequency, a simple passive bias-T circuitry (as shown in figure 7.8) is needed to directly couple modulation signal to the laser diode. The operating current range, output power and voltage drop are reported in figure 7.6 for a typical VCSEL source.

Temperature control of the laser diode must be stable within $0.01K$ during the measurement averaging time (ranging from fraction of seconds to minutes) to prevent waveform jittering. The effect of temperature control current on emission from a VCSEL diode is shown in figure 7.5. For lower powered VCSEL

Figure 7.4: A very common VCSEL laser diode driver suitable for both direct and WMS TDLAS. The left part of the board is the low noise current driver/modulator while the right one provides drive for the thermal control loop.

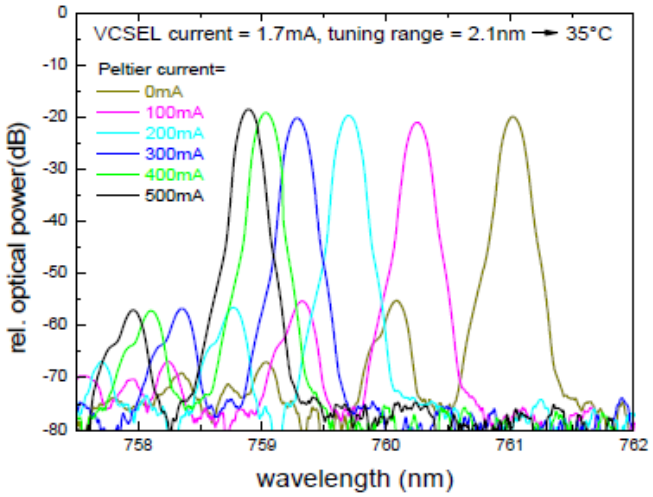

Figure 7.5: VCSEL diode emission spectrum at different temperatures, showing tunability.

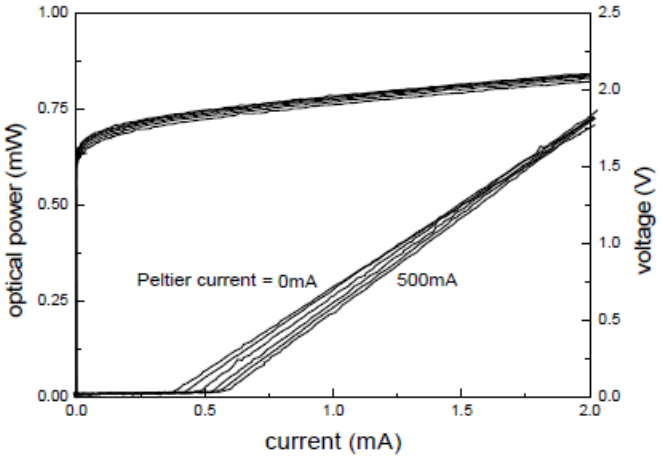

Figure 7.6: Junction voltage drop and emitted optical power as a function of forward current for a VCSEL diode.

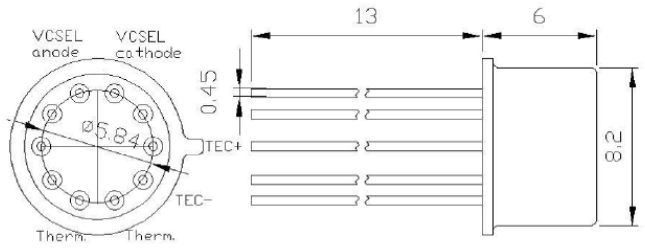

Figure 7.7: Typical TO5 VCSEL casing and pinout.

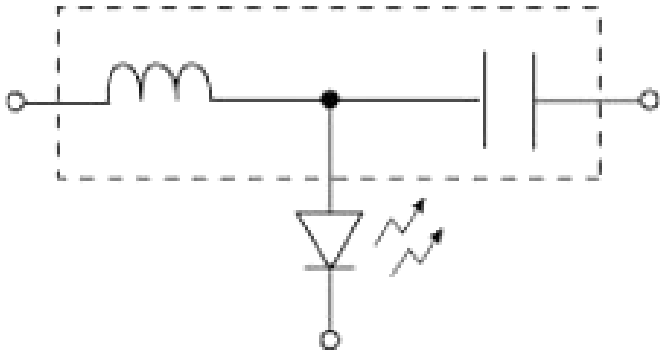

Figure 7.8: Simplified bias-T schematics (without protection diodes). Left branch is for scanning bias, right for modulation coupling.

devices the main source of temperature wandering was found to be related to thermistor positioning on the die and its heat exchanges with the external ambient. A good thermal contact of the surrounding mount with the casing and connecting pins (shown in figure 7.7) must be accomplished to help mitigating those effects. On DFB lasers even the variable heating contribution due to wide current scanning is not negligible.

7.1.2 Receiver end

Various photodetectors were found to be suitable to different applications. 760nm light can be easily detected with high responsivity by inexpensive silicon photodiodes. Those detectors can be readily found with different shapes and active area sizes, even quite large ($100mm^2$) ones. For applications where optical geometry may vary, even arrays of raw silicon photodiodes may be used.

Some of the used photodetectors:

- Thorlabs PDA36A preamplified Si photodiode with switchable gain, 3.6mm× 3.6mm (only for first experimentation due to lack of direct access to transimpedance gain stage;
- Hamamatsu S1337 series large area Si photodiodes, 6mm × 6mm and 10mm × 10mm;
- Hamamatsu S4111-35Q 35-element raw Si photodiode array, 35mm×4mm;
- BPW34 industry standard Si photodiode, 2.6mm × 2.6mm.

Large areas are useful for experiments involving scattering optical elements, but care must be put to avoid saturation by external lighting in high gain setups. Some kind of fluorescent lighting (both CFD lamps and traditional fluorescent ones with electronic ballasts) are known to generate electrical interference in the 100kHz range that may degrade signal-to-noise ratio. In most environments a Kodak Wratten gelatin filter can be helpful in mitigating this effect; the #29 deep red is a longpass type with a transition band from 600 to 700nm. Interference filters are not useful for this applications nor recomended due to their high incidence angle sensitivity and possible etalon behaviour interfering with the associated substrate layer. From a modulation point of view, longer integration time and spectral compression of the measurement signal band can be helpful in rejecting external noise sources.

Since in a WMS scheme the useful signal is only contained around the carrier frequency ω_m and its harmonics, the photodetector amplifier can take advantage of band-pass filtering to make better usage of its dynamic range, cutting out the very large DC signal from average laser power as well as the large linear scanning ramp.

7.1.3 Digital to analog to digital conversion

To improve noise and interference rejection by signal averaging and to avoid the complexity of an external reference oscillator channel with all the required circuitry, our digital WMS setup is always based on a synchronous D/A and A/D conversion respectively for laser driving and signal acquisition (figure 7.9). The board used in our prototypes is a National Instruments USB-6251 16-Bit, 1.25MS/s multifunction DAQ. This device may be configured to have both the ADC and DAC running off the same clock and sharing the same triggering signal. As an additional feature, there are digital I/Os that can be useful to control laser board interlock and switches, to sense laser board status signals and to control programmable photodetector amplifier (when required). The DAQ board is driven by a PC via a real-time (partially buffered) USB link.

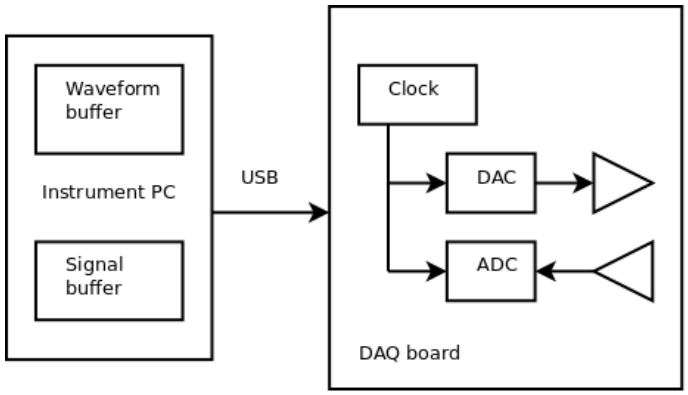

Figure 7.9: Block diagram of the DAQ setup.

The synchronous approach enables a fully software-defined modulation demodulation scheme, thus avoiding the requirement of a further phase detection and minimizing artifacts due to jitter and time dependent drifts. This greatly improves stability, allowing experiments to run for long integration times if re-

quired.

7.1.4 Instrument firmware

All the code for WMS instruments running on National Instruments DAQ boards was developed. The DAQ section was written in C language to achieve maximum speed even while running on low performance embedded PCs. A MATLAB version of the data processing section was also coded, to allow easier portability and tailoring in a lab environement.

The signal processing software running on the PC connected to the DAQ board is written to fulfill the following fundamental requirements:

- taking care of the digital IO signals for instrument control;
- filling the DAC buffer with the modulation waveform, digitally synthesized by summing a single triangular scanning period with an integer number of periods of the high-frequency modulation sine wave and a DC component for fine tuning of the laser center wavelength;
- triggering both the DAC and the ADC sections to run off the same clock;
- dumping the ADC buffer into a temporary memory space;
- iterating the previous steps a number of times, summing the ADC buffer data into the same memory space every time to average the acquired signal;
- normalizing the acquired signal to its RMS amplitude;
- calculating the FFT of the acquired signal;
- multiplying it by a supergaussian filter pulse response's FFT;
- shifting the resulting data to baseband;
- calculating the IFFT;
- applying the correct phase rotation;
- evaluating the output signal.

The main required input parameters for the code are:

- Number of scans to average;
- Amplitude of the sine wave modulation signal;
- Amplitude of the triangular scanning ramp;
- DC signal to fine tune the center wavelength to absorption line;
- Integer number of modulation periods in a scanning period;
- Number of samples in a scanning period;
- Sampling frequency;
- Demodulation index (harmonic order);
- Demodulation filter parameters (bandwidth);
- Phase angle.

Supergaussian filter

The supergaussian filter shape is chosen to have a steep frequency roll-off while maintaining a flat frequency in passband region. Another important feature of this filter is the shape preserving pulse response, causing no output overshoot. This is useful to avoid errors in the signal interpretation stage. An example of filtered signals affected by noise is shown in figure 7.10.

The frequency response for the supergaussian filter is given by:

$$G(\omega) = \mathcal{F}(g(t)) = e^{-(\frac{\omega - n\omega_m}{\delta\omega})^8} \tag{7.1}$$

where n is the chosen demodulation index, ω_m is the modulation carrier frequency and $\delta\omega$ is the filter bandwidth.

Data interpretation

After the demodulation and filtering, the output signal is stored in a data file for further processing. This step can be tailored in different ways depending on the specific application of the instrument (known pressure - pressure range, very noisy signal detection, strong interference).

Matched filtering

A very common technique for filtering a signal containing a pulse of known shape is matched filtering. This is particularly used in communication systems e. g. for decoding data from a PAM signal.

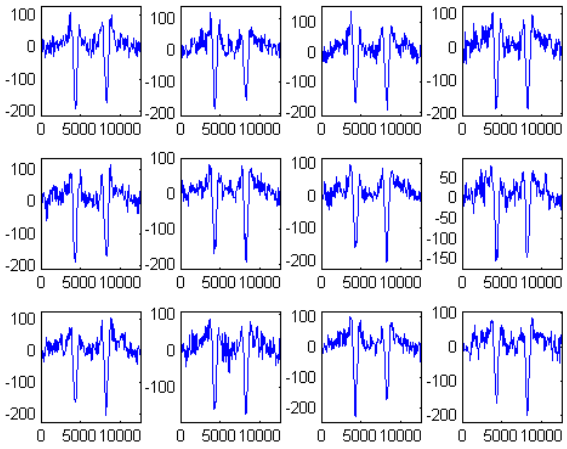

Figure 7.10: Example of lowpass WMS signals.

This is done by convolving the signal with a conjugated time reversed version of the pulse template. Such a linear-time-invariant filter can be shown to be the one which maximizes the signal-to-noise ratio in presence of additive stochastic noise. From a frequency domain point of view, this kind of filtering offers the greatest weighting to the spectral components with greater signal-to-noise ratio, resulting in signal such as the ones in figure 7.11 from the same input data of figure 7.10.

When the pulse template is an approximation of the acquired signal, the increase in signal-to-noise ratio is sub-optimal but the result is very predictable. This is a useful feature if compared to traditional least-square fitting techniques, which can give poor results with badly approximated models.

In WMS signal filtering, for example, we can use the simple n^{th} analytical derivative of a lorentzian function as a pulse template: if the modulation depth is non negligible, or if the pressure broadening is slightly different from expected, the signal output of a matched filter could be still better than the one obtained

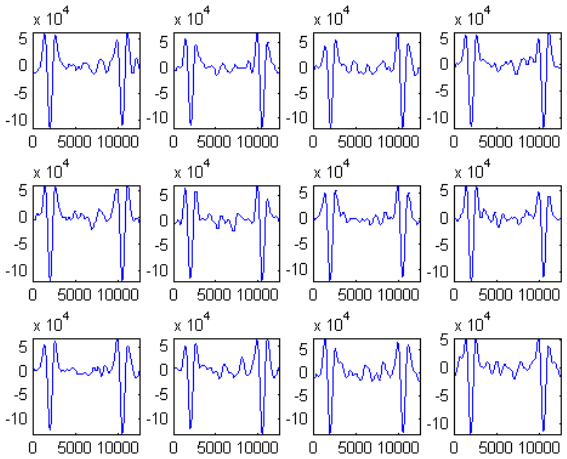

Figure 7.11: Example of WMS signals conditioned with matched filter.

by least-square fitting the experimental signal with the same model.

After filtering, the measurements parameters may be obtained from the output signal by evaluating peak-to-peak amplitude and width with simple algorithms.

Least-square fitting

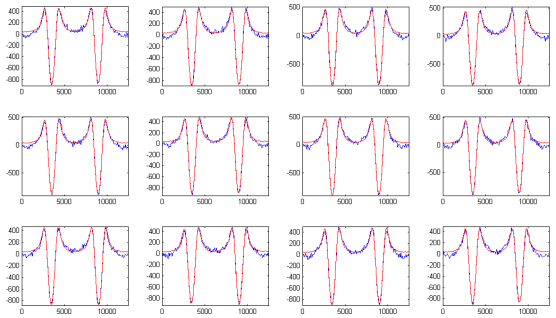

Figure 7.12: Least-square fitting of noisy WMS signals.

Another method for interpretation of the demodulated WMS signal is traditional least-square fitting. Of course, every fitting technique require a good

model. Even though an experimental waveform can be used as a model as well as a numerical approximation, it is important to point out that slight systematic errors in the model can make the algorithm to behave in an unpredictable way.

When a fitting algorithm is used, output amplitude and width parameters are automatically obtained as the model's parameters. The resulting signal is virtually noise-free, as shown in figure 7.12.

7.2 GASMAS

The ability of TDLAS to resolve gas absorption lines over broadband absorption coming from solid or liquid matter opens this technology to the detection of gases dispersed in non homogeneous media. This technique is called Gas in Scattering Media Absorption Spectroscopy (GASMAS) and while technically similar to regular TDLAS except for the non homogeneous (for example porous) sample, has the important difference that optical sample path length is unknown. For this reason it is impossible to apply the Lambert Beer law in a conventional manner as to extract a concentration value; the sample path length must be derived by a second measurement such as:

- A time-of-flight measurement system can be used in the same optical channel (at the same wavelength to maintain the same scattering behaviour)
- A reference gas at known concentration can be probed with another GASMAS channel, provided that absorption features are available at a close enough wavelength.

Chapter 8

WMS measurement systems

8.1 Oxygen measurement in closed glass bottles

In this section a system for oxygen detection in headspace of closed bottles will be described.

The wine bottling industry takes great care in monitoring dissolved oxygen in every step during wine processing, as oxidation is a detrimental factor in wine aging. Industrially produced wine is also provided with additives to take care of residual oxygen content. The amount of dissolved oxygen directly affects the shelf life of the bottled product; for this reason the whole raw wine handling and bottling is done in nitrogen flushed atmosphere. After the processing step, cork tightness is critical for correct preservation of wine.

Due to the forementioned reasons, an instrument for measuring gaseous oxygen in the headspace of wine bottles can be of large interest because it could even provide data about the equilibrium status between gaseous and dissolved phase (for example before and after shaking a sample). Of course, the other great feature of such an instrument is the non invasivity, enabling prolonged monitoring of the same set of samples.

Depending on the care used during the bottling process, the oxygen amount contained in the headspace can range from close to 20% to 2% just after bottling. Pressure ranges are from 0.6 to about 3 bar, on different bottling machine designs.

Equilibrium between gaseous and dissolved oxygen is given by Henry's law:

$$p = k_h c$$

where p is the partial pressure of the solute gas above the solution, k_h is the Henry's law constant (and is a function of gas, solvent and temperature) and c is the solute concentration in the solution.

As a reference figure, for fresh water in equilibrium the oxygen solubility is about $43 \frac{mg}{L \cdot bar}$ at a temperature of $20°C$.

The current techniques used in wine industry are both invasive and semi-invasive:

- gas sampling and chemical/electrochemical analysis;
- semi-invasive analysis in samples provided with fluorescence quenching.

Fluorescence quenching is a technique that involves a fluorophore (usually a ruthenium compound) trapped in a permeable media which is placed in contact with the sample. This fluorophore compound fluoresces when excited by a pump signal, such light coming from a blue LED. When interacting with an oxygen molecule from the sample (which can be in gaseous or liquid state) the excess energy quenches the fluorescence. An example of the layout used for a fluorescence quenching measurement is shown in figure 8.1. Both fluorescence intensity or fluorescence phase shift can be measured to determine oxygen concentration. The intensity measurement is usually more prone to drifts and sensitivity to degrading of the fluorophore, while the phase measurement can be more robust at the expense of requiring more complex electronics and a pump source which can be pulsed usually in the kHz range.

8.1.1 Optical configuration

The system discussed in this part (shown in figure 8.2) has been tested and made to work on common dark glass wine bottles. This required an optical configuration designed to take account of a sample container (the neck of a bottle) which is far from perfect being made of rough, dark glass. The imperfections of the material provide scattering sources and strong back-reflections restricting the suitable range of laser cavities to only VCSEL devices, which are provided with high reflectivity mirrors on the chip making them less sensitive to self-mixing.

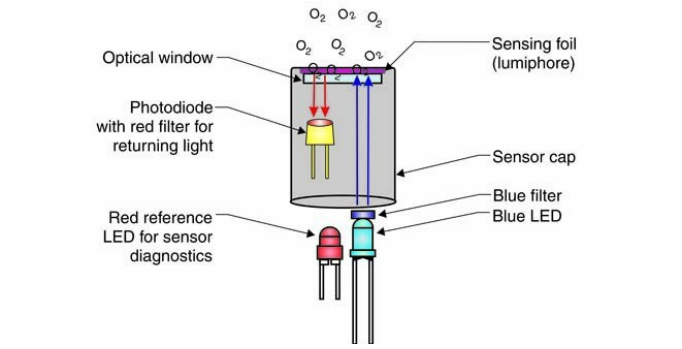

Figure 8.1: Schematics of a commercial Fluorescence Quenching oxygen sensor.

Another challenge of this application has been the unknown pressure of the sample which differs from ambient air: different types of wine or beverage and different corking machines can cause the headspace pressure to be between 0.5 and 8 bar. Considering the low oxygen content (even under 1%) inside the bottle compared to external air path, it can be very difficult to separate the two absorption signals. To solve this problem, we developed transparent silicone rubber gaskets to make an air free optical contact with the sample bottle (figure 8.3). This has the additional feature of partially matching the refractive index between optical surfaces and reducing back reflections, as the selected silicone rubber has a refractive index about 1.4.

To take care of residual interferometric effects, a vibration motor has been included in the optical mount to randomly dither cavity length and accomplish interference-to-noise conversion.

For this experiment the laser beam has been left uncollimated to avoid any additional optics and to average out imperfections on the glass bottle. This required a large-area photodiode on the receiver side, but the resulting system is not influenced by optical and geometrical defects of the sample. Due to the low and variable amount of received power, a programmable gain amplifier was designed and built. The schematics and printed circuit board layout are shown in figure 8.4 and 8.5.

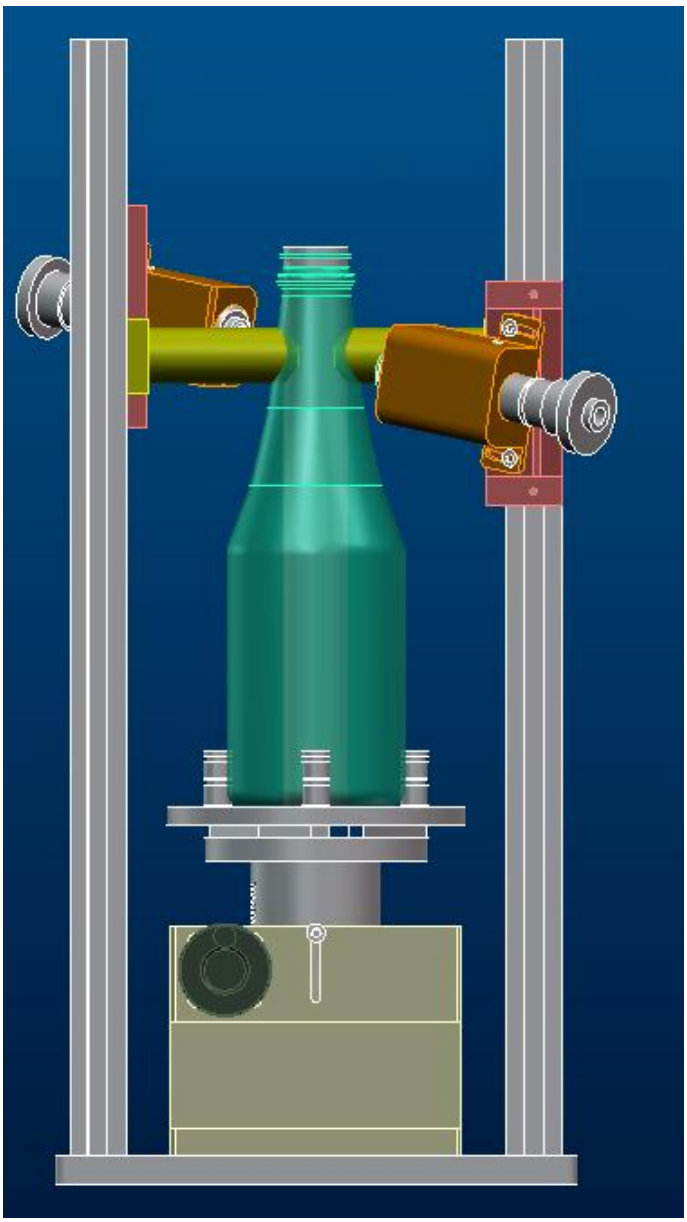

Figure 8.2: Layout of the combined oxygen and carbon dioxide analyzer prototype.

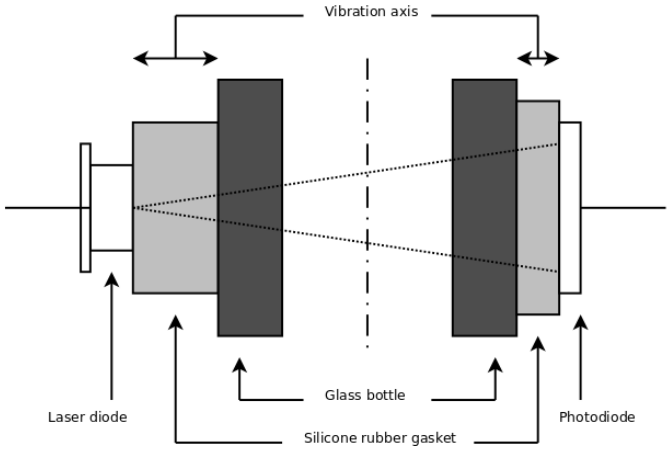

Figure 8.3: Optical layout with transparent silicone rubber gaskets.

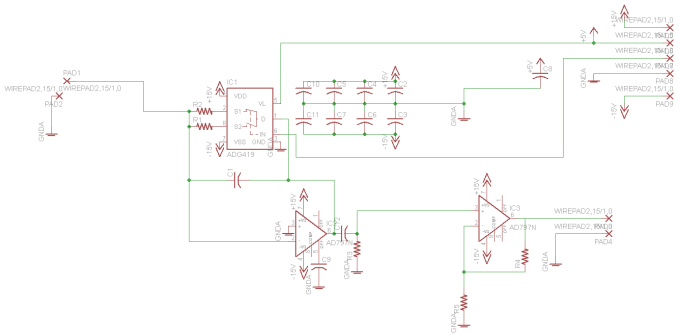

Figure 8.4: Schematics of the programmable transimpedance gain amplifier designed for the application.

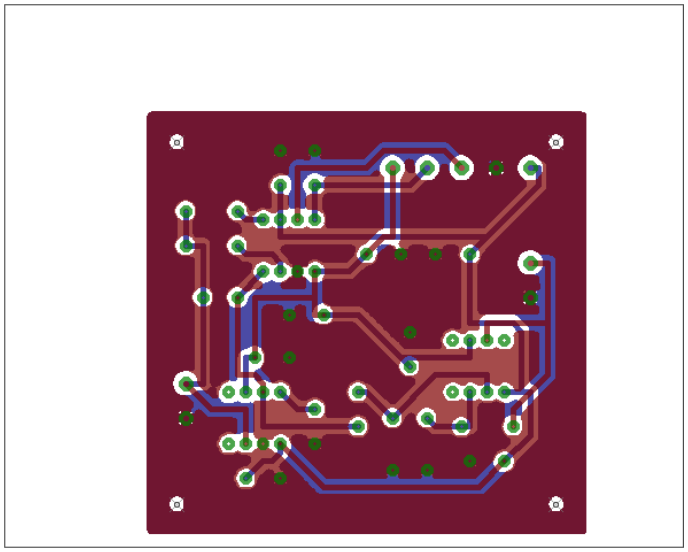

Figure 8.5: Board layout of the programmable transimpedance gain amplifier built for the application.

8.1.2 Measurement interpretation

Because of the very low optical power (μW range) emerging from the sample, a pressure measurement based on the only oxygen absorption trace can be very noisy if the oxygen concentration is low. In this case, it is possible to use a different wavelength TDLAS setup to estimate sample pressure through measurement of a strong absorption line from another molecule inside the sample. For example, pressure measurement on CO_2 absorption lines around $2\mu m$ inside wine bottles can give very accurate results. Thanks to this, it is possible to use a calibration curve, as shown in figure 8.6, to take account of different instrument response for oxygen monitoring channel as a function of pressure.

Carbon dioxide, which is always present in wine bottles being a fermentation byproduct, is the preferred choice for pressure measurements due to a very strong absorption band near $2\mu m$ which usually requires no wavelength modulation at all to be evaluated.

Performance of the oxygen measurement channel can reach about 0.3% O_2 for atmospheric pressures, at the point where geometrical imperfections of a common glass bottle start to become significant. For that reason it could be useful to average together different measurements over different diameters of

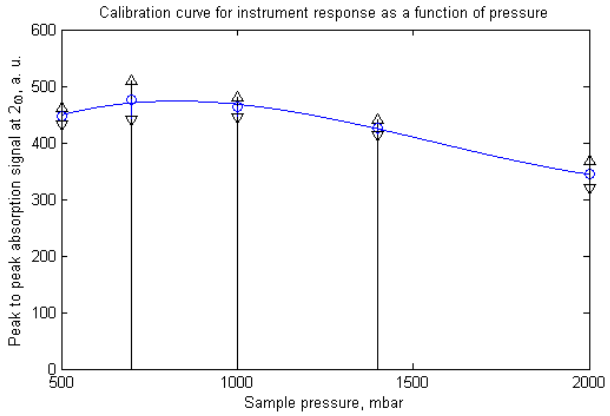

Figure 8.6: Calibration curve as a function of pressure enabling concentration measurements from 2ω WMS oxygen absorption signal.

the bottle.

The instrument performance was shown to improve proportionally with the square root of integration time at least up to several minutes. This is due both to the small optical signal received by the photodetector and the interference-to-noise conversion operated by dithering.

It is important to note that at higher pressures the performance degradation is about proportional with pressure, up to about 3 times the standard pressure (1 bar) for which the modulation parameters were optimized.

8.2 Oxygen measurement in double-glazing insulating glass

The current trends towards energy-saving in building techniques requires windows to be much more than a plain sheet of glass. Modern windows are usually made with double-glazing insulating glass filled with inert gases such as argon, kripton, xenon, sulfur hexafluoride.

Another improvement in double-glazing technology is represented by coated glass:

- to reflect the near-IR from the sun on the outside;
- to keep the blackbody IR from the inside.

Building codes require the filling gas purity to be evaluated and guaranteed for the entire life span of the panel. An instrument for measuring the amount of residual air in the panel, both as a test for the filling process and as a method for detecting leaks in the spacer sealant would be greatly appreciated by the glass industry.

This kind of measurement is now done in two ways:

- invasive sampling of the gas in a sacrifical sample and chemical lab analysis; this is the current requirement for certified glass, of course not useful for production line monitoring.

- corona discharge probes; the only non invasive method currently available, requires different probes for different filling gases and its accuracy and repetability are badly affected by coated glasses.

The optimal thickness of a glass panel is fixed, given a particular filling gas. Thermal performances of a glass with thinner than optimal gap are limited by conductive losses, while a thicker one will be impaired by convection losses. Considering air as a filling, the optimum is reached between $16 - 19mm$; this value becomes lower for argon and even lower for krypton filling. Soldered evacuated glasses are also found on the market, but the need for a rigid seal makes those panels very sensitive to thermal stresses, restricting them to applications where the temperature differential is below $35°C$.

8.2.1 Optical configuration

This instrument has been developed with the intention of both a quality control on glass production lines and a portable instrument for already mounted panels. For this reason, the instrument has been designed to work from a single side of the glass panel. The measurement has to be possible on a broad range of panel thicknesses.

The optical design works by sending an s-polarized, collimated beam impinging at around 60° from perpendicular to the glass plate. The beam is partly transmitted and partly reflected at each surface, giving back an array of spots as shown in figure 8.7 and 8.8.

Given the fixed refractive index of glass, the spot intensities are influenced by bulk absorption into glass and by the presence of coatings, which are usually

reflective. On the detector side, the collection of light after propagation through the sample is made by placing the detector on the correct spot. This has the advantage of avoiding optical interference between adjacent spots, as the spot size is smaller than minimum spacing for a system without interfaces thinner than $3mm$.

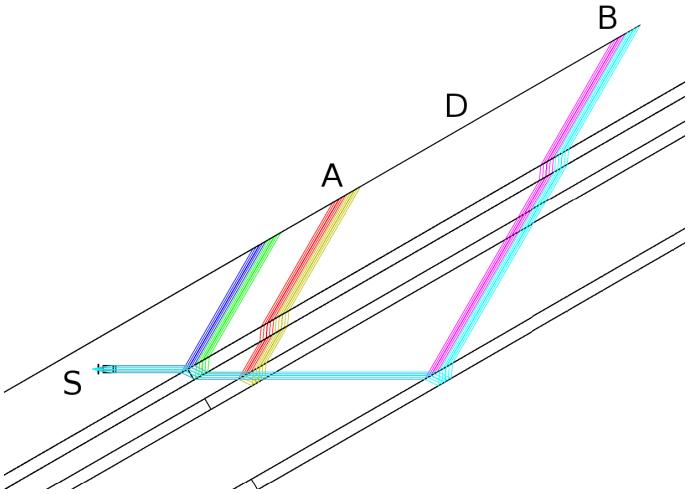

Figure 8.7: Optical layout for different gap thicknesses (6 and $32mm$). Useful measurement rays are A ($6mm$) and B ($32mm$). Detector is moving on plane D and source is placed in S.

Figure 8.8: Spot diagram for Figure 8.7.

On the source side, light from a thermally controlled VCSEL source (ULM photonics ULM760-01-TN-S46FTT) is collimated with an aspheric lens (Rochester A230) mounted on a flexural pivot (shown in figure 8.10). The elastic lens mount is energized with a vibrating electric motor operating around 200Hz to provide beam dithering and cancel stray optical interference. The light collection assembly is made by a Si-PIN photodiode (BPW54) mounted on a mechanical translation stage (figure 8.11).

The instrument has to be able to detect oxygen concentrations below 1% with

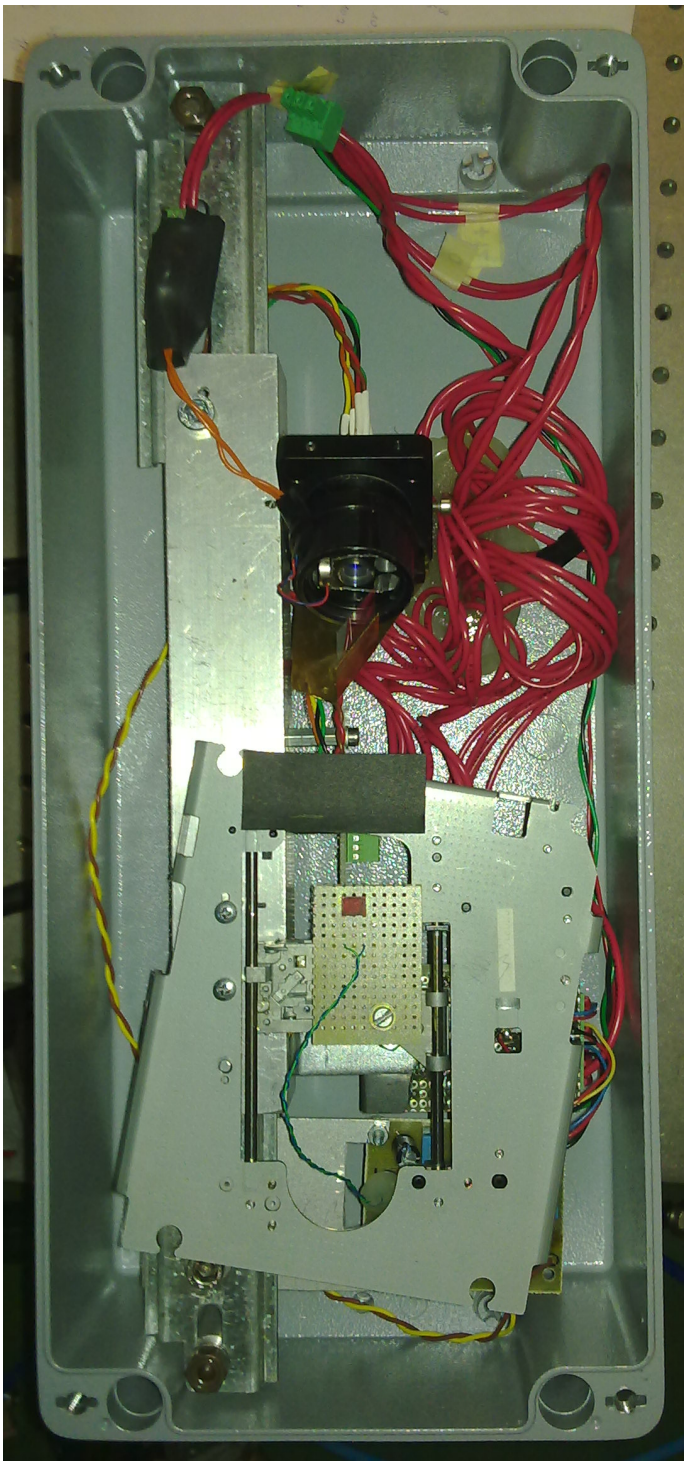

Figure 8.9: Prototype insides, showing laser source (top) and detector on translation stage (bottom).

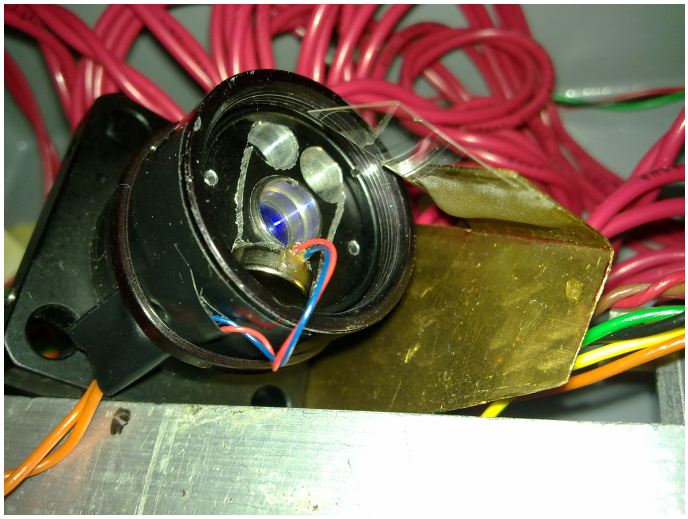

Figure 8.10: Laser source assembly, showing collimation lens on flexural pivot vibrating mount.

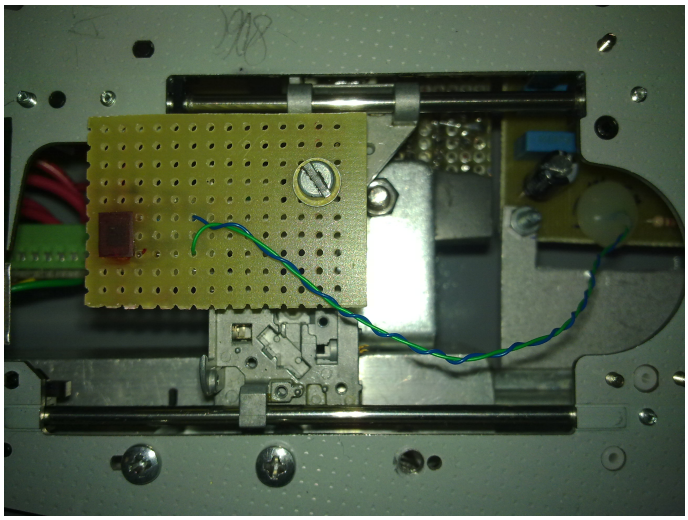

Figure 8.11: Photodiode assembly, showing translation stage (foreground), translation controller and photodiode amplifier board (background).

the typical glass having a gap thickness of just 12mm. To allow such sensitivity it is mandatory to avoid adding any external (ambient) air contribution to the optical path. The designed measurement head is contained in a gas-tight box flushed with nitrogen and provided with an oxygen scavenger (iron powder) bag. Optical contact with the sample is provided through a transparent side of the box, while the opposite side is provided with sealed electrical feed-through for the source and detector circuitry. An overall view of the instrument insides is shown in figure 8.9.

8.2.2 Translation stage

The mechanical translation stage, derived from a CD player head, provides a $40mm$ stroke with $0.1mm$ step resolution.

On the hardware side the stage features a moving carriage riding on two guides and driven by a leadscrew. Backlash compensation is done by elastic mounts. The leadscrew movement is done by a DC motor coupled by a gear train. There are also a relative optical encoder on the motor shaft and a limit switch provided as means for accurate carriage positioning.

8.2.3 Instrument operation

To provide compatibility with most types of glass panels, a photodiode alignment routine (which is described in figure 8.12) is provided with the instrument. The scanning utility does a measurement of received optical power as a function of photodiode position (leading to a distribution similar to the example reported in figure 8.13) and detects the peak coming from the first reflection at the inner glass surface opposite to the instrument (rightmost in figure 8.13).

The scanning utility does not need to be run before every measurement; to speed up the measurement time the user can provide the photodiode position manually once the scanning is done for a given type of glass. Correct photodiode positioning depends upon both the thicknesses of the instrument-side glass and the gas gap, but is not as sensitive to require realignments due to each glass panel manufacturing tolerances.

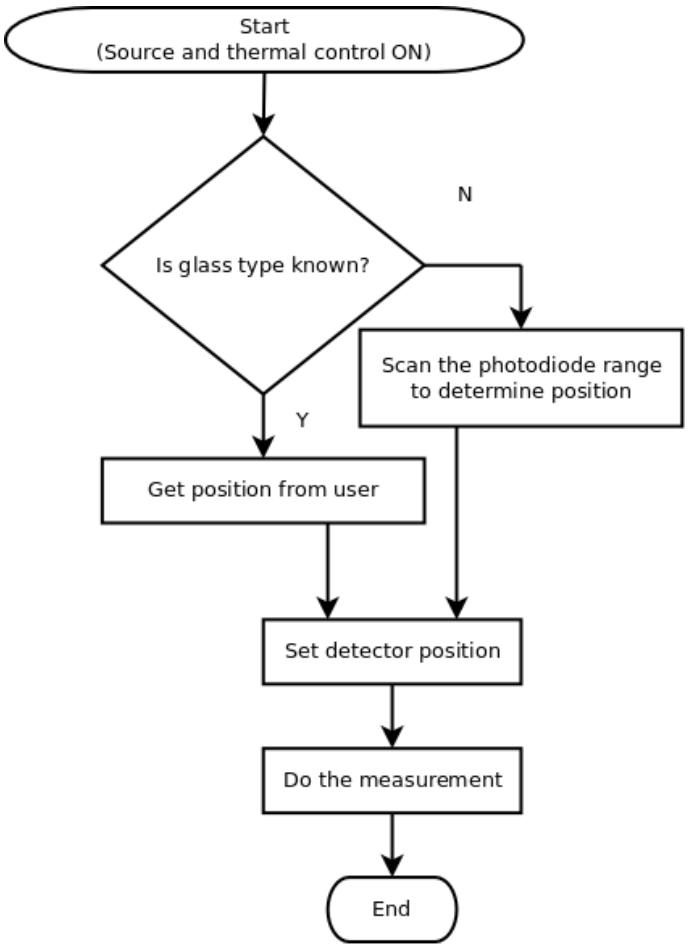

Figure 8.12: Simplified flow chart representing instrument operation.

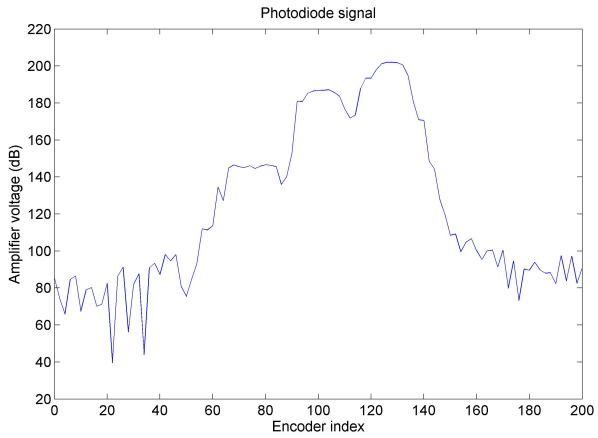

Figure 8.13: Photodiode signal as a function of position for a standard double 4mm glass with 12mm gas gap, showing useful peak (rightmost) and stray reflections (on the left).

8.2.4 Results

The instrument response was tested for linearity using a 12mm thick reference cell which can be flushed with known gas mixtures prepared in a separate tank. The observed linearity is excellent, well below other causes of errors that can influence a measurement as shown in figure 8.14.

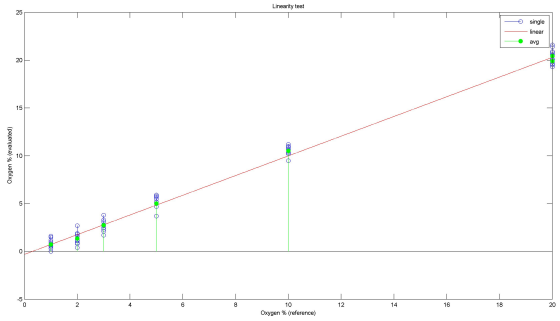

Figure 8.14: Measurements of known gas mixtures in a cell, with linear fit. Worst case of transparent glass.

The instrument was tested against a sampling of common glass panels of

different kinds:

- transparent (or far-IR coated);
- near-IR coated;
- laminated;
- toughened.

Repetability was found to be better on coated glasses; this can be explained considering the lower intensity of stray reflection compared to the useful reflection, giving a lower stray etalon effect. A comparison of the demodulated signals obtained with coated and uncoated glass is reported in figures 8.15 and 8.16.

Instrument operation with short integration times such as 250ms, 500ms and 1s was tried to prove the feasibility of a dynamic monitoring of the gas filling process, which usually takes a few seconds. Figure 8.17 clearly shows the instrument ability to resolve such transients and evaluate the filling process with fast response times.

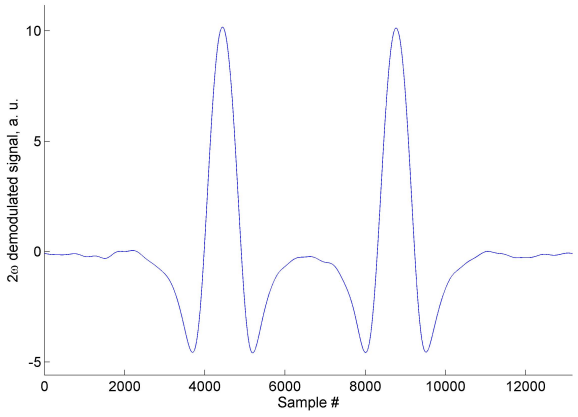

Figure 8.15: 2ω WMS signal from a coated glass filled with air.

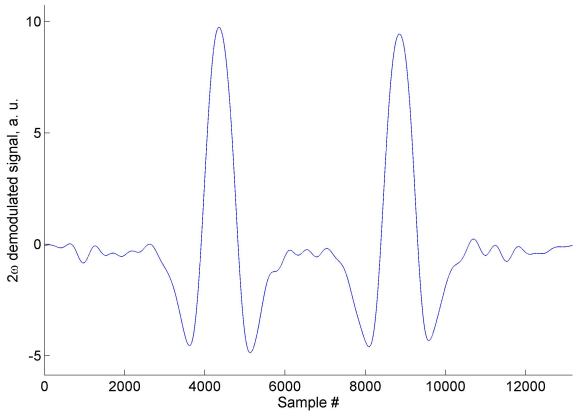

Figure 8.16: 2ω WMS signal from a transparent glass filled with air.

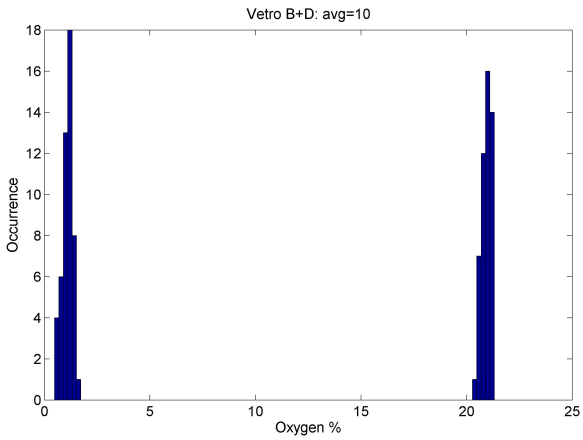

Figure 8.17: Histogram representing evaluated concentrations for a sealed glass and for an open one. Integration time is 500ms, showing that the instrument could be used also for line-monitoring of gas filling equipment.

8.3 Oxygen measurement in food packaging

8.3.1 Optical configuration

This system has been set up to make measurements in food packing trays which are made by an opaque container closed by a welded transparent film on the top surface. It is not possible to find a transmission optical path through this type of container, so the measurement has to be done on back-reflected light coming from the bottom of the container or the food itself. A 1/4" CMOS, 9mm focal

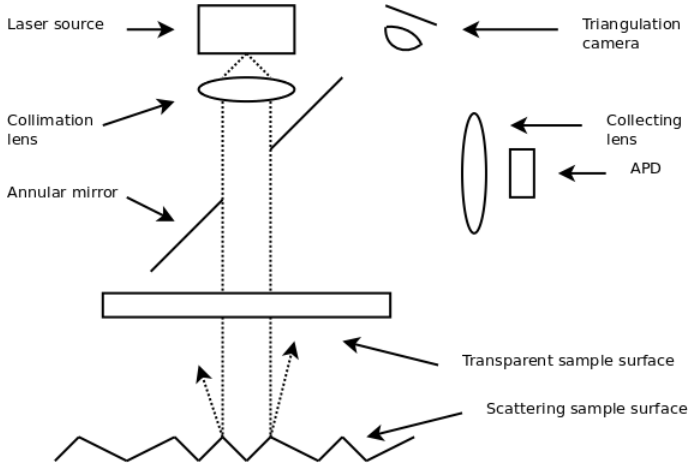

Figure 8.18: Simplified optical configuration schematics.

length camera is provided within the instrument, observing the spot image on the scattering surface off-axis to determine spot position through triangulation. This measurements allows application of the Beer Lambert law for resolving oxygen concentration. The optical layout is shown in figure 8.18.

Due to the long optical path of the instrument internals, a gas-tight oxygen-free enclosure was assembled and provided with oxygen scavengers to ensure a direct sample measurement without influence of the external oxygen concentration.

The optical interface between instrument and sample is contained in a quasi rectangular area sized $10 \times 5mm^2$, closed with an AR-coated plexiglass window.

Interference-to-noise conversion is provided by two vibrating motors:

- on the laser collimating lens mount through a flexural pivot;

- on the sample table.

The triangulation distance meter provides a distance measurement through imaging of the same measurement spot on the sample. Focus of the camera is fixed mid-way through the allowed measuremt range, which is around 10 to 60mm. A centroid detection algorithm determines the spot position on the focal plane which is then related to scattering surface distance through a built-in calibration curve.

8.4 Residual pressure detection in vacuum impregnated apple samples

This part of work has been done together with Lunds Universitet - Lunds Tekniska Högskola - Atomfysik [4].

Vacuum impregnation is a technique used in food industry to fill porosities of a material with a liquid. This method is used on apples into isotonic sugar solution mainly to raise specific gravity of apple pieces in order to pump the whole suspension as a fluid. Apple pieces are immersed in isotonic solution and vacuum is applied gradually, to avoid mechanical collapse of the fruit structure and consequent degradation in texture. This replaces with fluid the greatest part of gas trapped into pores.

The microstructure and the capillary pressure of the pore space are important variables for better understanding of the complex phenomena occurring during vacuum impregnation (VI) of plant tissues. In this study, we used GASMAS (Gas in Scattering Media Absorption Spectroscopy) of oxygen to, non-destructively, measure the dynamics of the internal pressure in apple pieces after restoration of the atmospheric pressure. Apple pieces were impregnated with isotonic sucrose solution (18% w/v) at different reduced pressures (15, 30, 45 kPa (abs)). After restoration of the atmospheric pressure, the pressure of the remaining pore space gas could remain as low as 50 kPa (abs) and rise slowly toward ambient over a time scale of hours. Both the residual vacuum and the timescale of pressure equilibration with ambient varied with applied vacuum level and apple variety. It is proposed that at least a part of the pore space of apples may be hydrophobic, giving rise to a negative Laplace pressure, and thus the convective flow of impregnating solution is arrested at a mechanical

equilibrium where internal pressure is lower than external pressure. Further pressure equilibration can then only be achieved either by gas diffusion in gas phase, or by gradual wetting of the pores.

The GASMAS instrument consisted in a Toptica DFB laser diode, scanning an oxygen absorption line around 760nm with about 30mW of output power. The laser diode was contained in a TEC thermally controlled module (Thorlabs TCLDM9); a 10mm nitrogen flushed gas spacer was placed in front of the diverging laser beam both to reduce interference from backscattered light and to avoid thermal drifts induced by conduction from the sample to the laser mount.

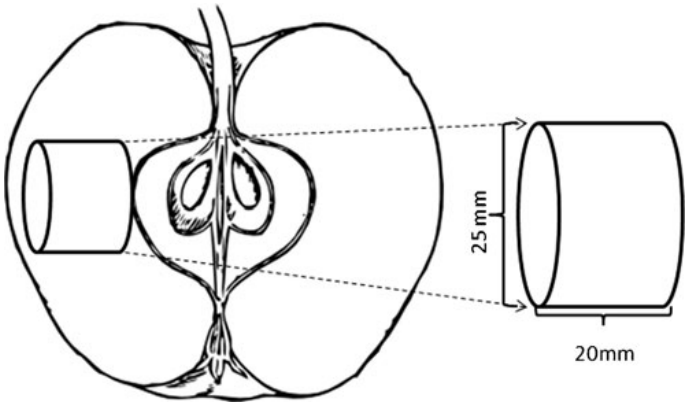

Figure 8.19: Dimensional sketch of apple samples.

The apple sample is a radially cut cylinder 25mm in diameter by 20mm in length as shown in figure 8.19, obtained by core sampling of a skinned apple. This is needed to achieve the most homogenous sampling from samples which are, by nature, dishomogeneous.

At the detector side we used a large-area, $10 \times 10mm^2$ photodiode (Hamamatsu S3590-01) to collect light emerging from the sample. Layout is shown in figure 8.20.

8.4.1 Reference experiment

Even though a numerical model of the WMS signal can be built for any kind of modulation and absorption line, a model of the laser output response for a given modulation can be very difficult to obtain, due to varying amplitude and wavelength modulation efficiency in the sweep range. An easier way to evaluate

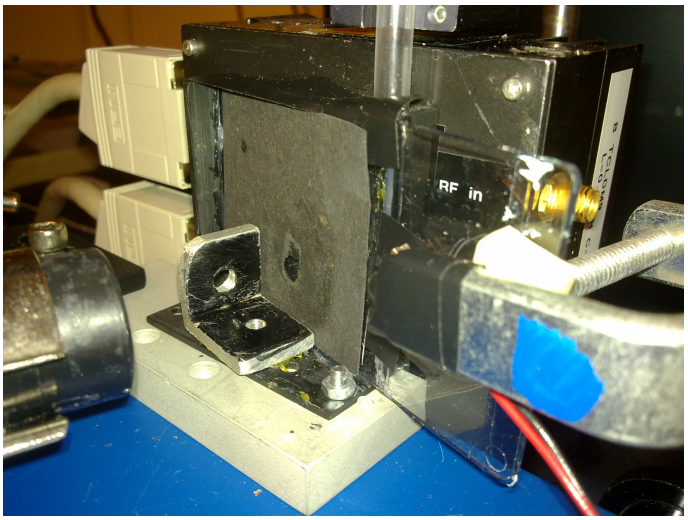

Figure 8.20: GASMAS optical setup for apple samples; detector on the left, laser diode mount on the right.

WMS signals in a varying pressure broadening condition needs a set of reference signals for fitting and comparison.

To enable pressure measurement by evaluation of line broadening from apple WMS data a second experiment was set up. The purpouse of this was to record noise-free WMS reference waveforms from a known-pressure oxygen absorption path.

The same source and detector as in the apple measurements were separated by a $90cm$ long gas cell, with wedged optical windows at both sides. A vacuum pump was connected to the gas cell through a needle valve and pressure in the cell was measured with a manometer. This setup was used to acquire corresponding signals for the range 133hPa to 1000hPa with 33hPa step resolution. The result is shown in figure 8.21.

8.4.2 Signal evaluation technique

The usual method for detecting concentration from a WMS signal consists in fitting (e. g. least-square minimization) the experimental signal with a scaled known reference, which could be both experimental or the result of a numerical simulation. This approach is limited by the need of having both the reference

and the experimental samples at the same pressure and temperature. This is required for the fitting operation to be meaningful.

In the case of unknown pressure at the sample, the fitting has been tried with all the reference signal. The sum of squares of the residual signal (difference between fitted and experimental data) has been used as a measure of "how representative" is the reference data respect to the experimental signal.

At this point sample pressure is simply assumed to be the one of the reference data that returned the least amount of residual.

However, considering the apple experiment, the whole idea of pressure has to be discussed. By detecting residual gas after VI process, we are intrinsically assuming there are closed pores and/or significant head losses between pores; it is not obvious to assume the pores at the same pressure.

An advantage of the described method stands in proving the correctness of this assumption at the same time. If the experimental data can be fitted with a model at a single pressure, returning residuals which are low in comparison with the experimental signal, then the contribution by oxygen absorption at pressures different from the measured one is negligible.

Another interesting issue to be discussed about pressure broadening in GAS-MAS is pore-size induced broadening. Pressure measurement with absorption linewidth are possible because the absorption profile is broadened by collisions between molecules, assuming that pore size is much larger than the mean free path of the considered molecule.

For reference, the mean free path for oxygen in ambient air is around $100nm$ at $300hPa$ and $20°C$.

If the pore size becomes much smaller than the mean free path, pore size itself could be measurable by linewidth.

8.4.3 Results

This experiment led to an interesting finding. If the air inside pores was not completely removed, the remaining part retained an "average" pressure lower than ambient, which recovered on a time scale of hours according to figure 8.22. Intuitively one could expect the pressure to increase with some sort of exponential behaviour. However, it is likely that such would then include more than one time constant as we have pores and channels of different sizes in the sample.

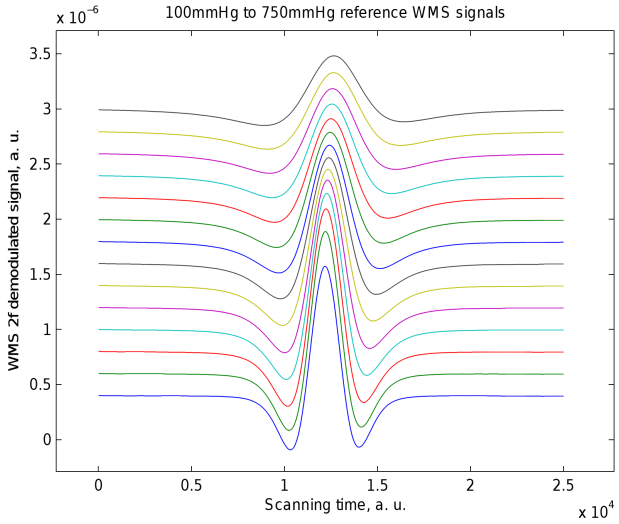

Figure 8.21: WMS pressure reference signals.

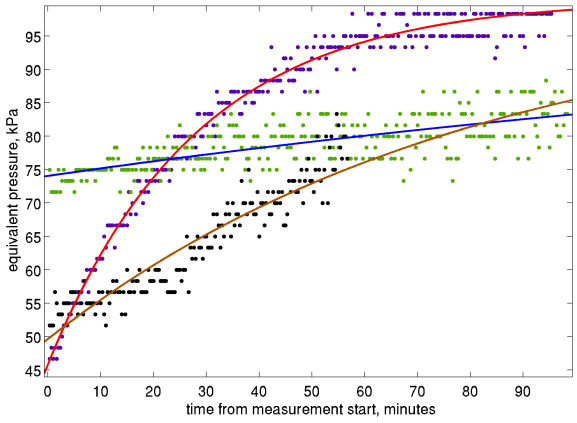

Figure 8.22: Pressure series from apple samples after vacuum impregnation.

To show that this delay effect depends on capillary pressure in the interconnections between pores another experiment was done. This time vacuum impregnation was accomplished with a "blank" sample not immersed in the isotonic solution. The result was an immediate pressure recovery, without any measurable transient.

8.5 Oxygen probing into human tissues

This part of work has been done together with Lunds Universitet - Lunds Tekniska Högskola - Atomfysik.

GASMAS can be applied to living human tissues for medical diagnosis; the importance of such measurements can be found in:

- Diagnosis of sinusitis by measurements on gases contained in the paranasal sinuses;
- Assessment of lung functionality in prematurely born babies.

As the cavities inside the human body can be sampled only with a GASMAS approach, the only way to evaluate oxygen concentrations is by comparison with a water vapour reference channel. Water vapour is assumed to be at saturation for body temperature, and can be sounded at 820nm or 935nm. The 820nm wavelength is preferrable to the 935nm one as the scattering properties are closer to the oxygen channel operating at 760nm, but can be more sensitive to noise as the line intensity is about 10 times lower.

The evaluated parameter used for diagnosis is a ratio between water and oxygen absorption signals: the reference scale should be determined by experience on the field on both healthy and diseased patients.

The two channels originating from different sources are fibers coupled together and the chosen modulation frequency is different for each one (around 9kHz and 10kHz), in order to do a proper multiplexing and effectively doing simultaneous but completely independent measurements. The photodetector choice is usually restricted to a large area photodiode, as the high voltages used in active gain detectors as APDs and PMTs are not compliant with safety standards of a medical environment. The signal processing scheme is still the traditional digital synchronous lock-in running on NI-DAQ boards and described in the other experiments discussed in this work.

8.6 Oxygen monitoring in scattering packages

Figure 8.23: Scattering packages made of multilayer paper and plastic are very common in milk, dairy products and juice packaging.

This part of work has been done together with Lunds Universitet - Lunds Tekniska Högskola - Atomfysik and Tetrapak.

Packaging is vital for keeping product quality and maintaining shelf-life of food. This is especially important for fresh and chilled products that are more sensitive to deterioration. Deterioration processes hasten by the presence of light and oxygen and also by temperature exposure. In order to slow down these processes, package headspaces are frequently filled with a modified atmosphere in order to reduce the oxygen content in direct contact with the packed food. The package integrity is therefore vital in order to avoid transmission of oxygen from the outside environment into the package headspace, and is thus a key parameter to monitor. Modified atmosphere packaging is a standard procedure in the food industry in order to increase the product shelf-life, to satisfy consumers requirements for fresh food, and to facilitate the constant strive for reducing material and product waste and to reduce transports, thus considering both economic and environmental aspects. Research in this field can gain great advantage from the availability of an instrument able to measure gas concentrations in a non-intrusive manner. In this way, food and packaging quality as well as aging can be assessed during the whole shelf-life of the product, without sample waste.

An instrument for WMS GASMAS has been developed. The light from the laser was illuminated onto one of the top surfaces of the package. The plastic material of the packages will reflect or absorb most of the light, but a small

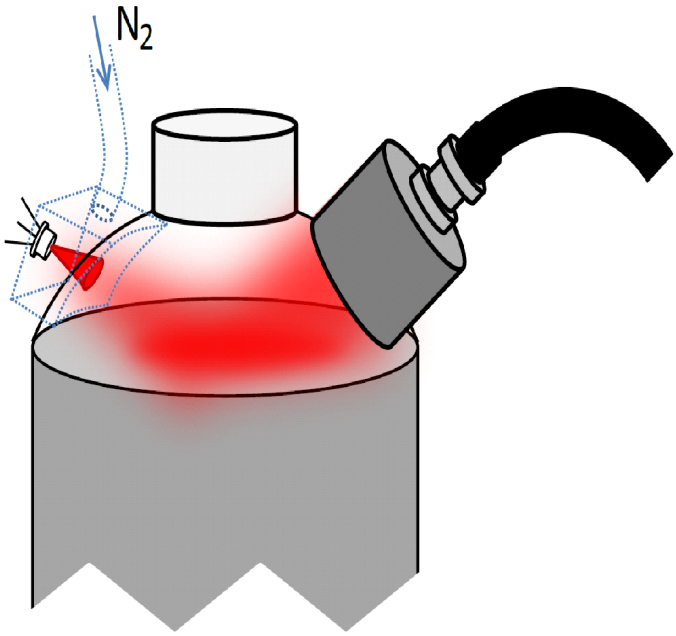

Figure 8.24: Detecting oxygen in Tetrapak containers through GASMAS.

fraction is diffusively transmitted through the plastic and into the package. The diffusely transmitted light will be scattered in the headspace before most is, again, absorbed by the plastic or liquid. However, a minor fraction of the total light will reach the detector (a large-area photo diode (PD), Hamamatsu, Model S3204-08, 18X18 mm^2, or Photomultiplier tube (PMT), Hamamatsu, Model R5070A, active diameter 23 mm) placed on the opposite side of the headspace. This layout is shown in figure 8.24. Even if most light is lost due to scattering and absorption by the solid material of the package and the liquid inside, any gas absorption in the light received by the detector is easily found due to the much more distinct and sharp features of a gas absorption imprint. To avoid the light absorption signal being affected by the atmosphere outside of the package, the short but unavoidable distance (5 mm) between the laser and the package is flushed with nitrogen gas. Further, to suppress interference effects in the light, which could potentially make the signal noisy, the laser mount was vibrated with a small cell phone vibrator. Since the path length of the light travelled inside the headspace is primarily unknown during a GASMAS measurement, the concentration cannot directly be retrieved from the absorption fraction. However, since packages of the same model are more or less identical we solve the problem by initially performing calibration measurements on packages with known concentration and from this calculate the effective path length of light travel inside each package model.

Our instrument was compared to a commercially available, invasive electrochemical oxygen sensor (PBI DanSensor, Model Checkmate 9900) on a sampling of packages provided by Tetrapak. The result, as reported in figure 8.26, shows good correlation between the two instruments. It is important to point out that operation of the invasive reference analyzer on so many measurements required frequent replacements of the piercing needle probe, as clogging by food contamination was found to be responsible of strong inaccuracies in the measurement.

The dynamic response of the instrument was also tested on package flushing transients (figure 8.25). Due to the low received signal and strong interference effects, time resolution is limited to the 10s range.

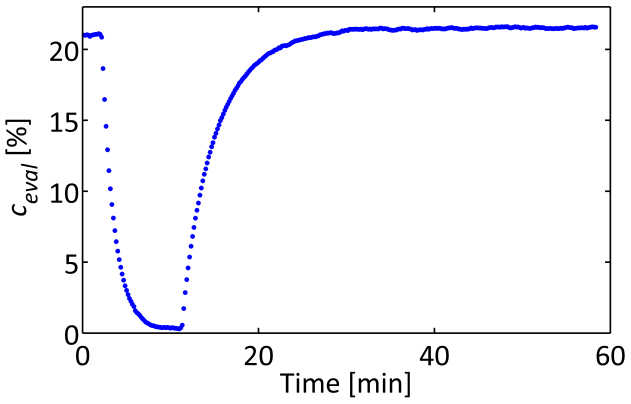

Figure 8.25: Example of oxygen concentration measurement as a function of time during and after nitrogen flushing on a pierced Tetrapak juice package, showing the instrument ability to dynamically resolve oxygen concentrations.

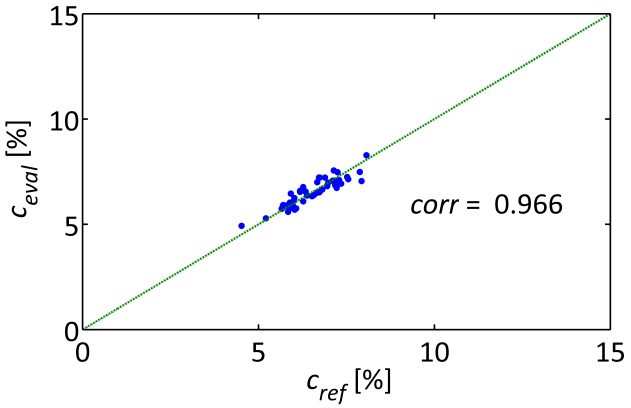

Figure 8.26: Result of instrument testing on many samples of Tetrapak juice packages, showing correlation with reference measurement provided by PBI DanSensor, Model Checkmate 9900.

8.7 Oven temperature measurement through multi-line oxygen WMS

This part of work has been done together with Lunds Universitet - Lunds Tekniska Högskola - Atomfysik as part of a proof-of-principle shown to SWEREA.

An experiment for showing air temperature measurement through WMS TDLAS has been set up in a common household oven. The experiment was meant to show the suitability of this technology for non invasive temperature monitoring in industrial (metallurgical) processes.

A VCSEL diode was chosen as the source because of its wide tunability, enabling fast scanning over 10 absorption lines in the 760nm band at a constant temperature. Ratios between absorption lines in the scanned band are known (from HITRAN simulations) to be strongly temperature dependent in the measurement range (20 to 200$°C$), as shown in figure 8.27 and 8.28.

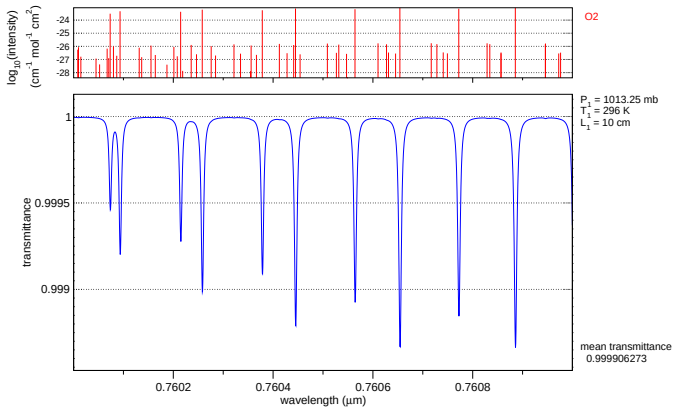

Figure 8.27: Part of the oxygen absorption spectrum at 296K.

The measurement beam was sent to a polished aluminium plate into the oven through the glass door and the back-reflected signal was collected by an external photodiode. Oven temperature was monitored with a K-type thermocouple and heat output was accurately controlled with a variac to provide stable temperatures.

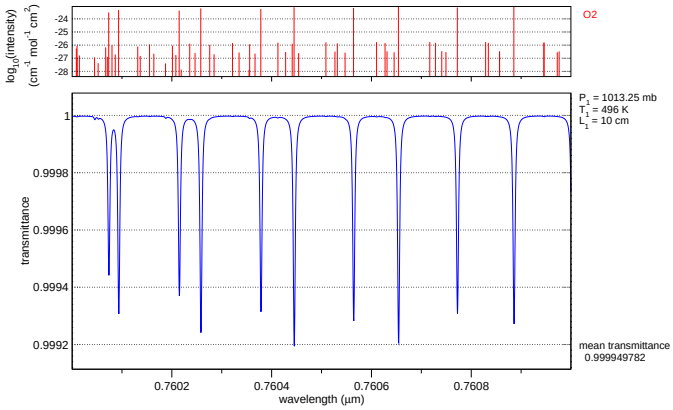

Figure 8.28: Part of the oxygen absorption spectrum at 496K.

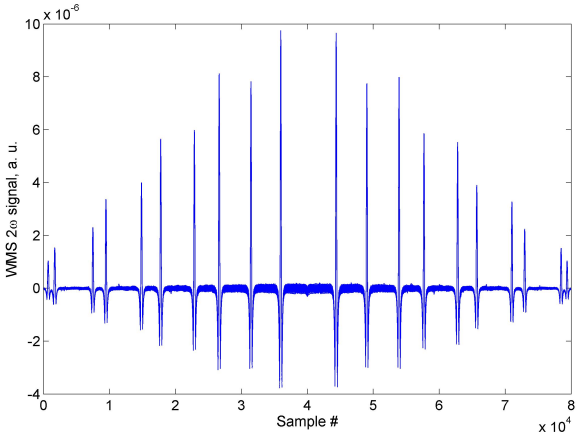

Figure 8.29: 2ω WMS signal, scanning over 10 lines.

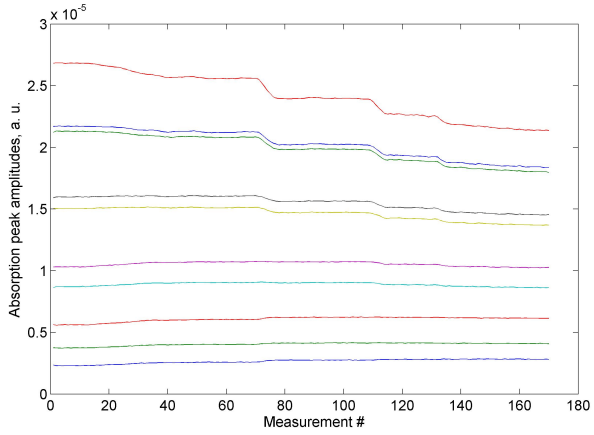

Figure 8.30: Amplitude behaviour of the 10 scanned lines during a 5-step temperature transient.

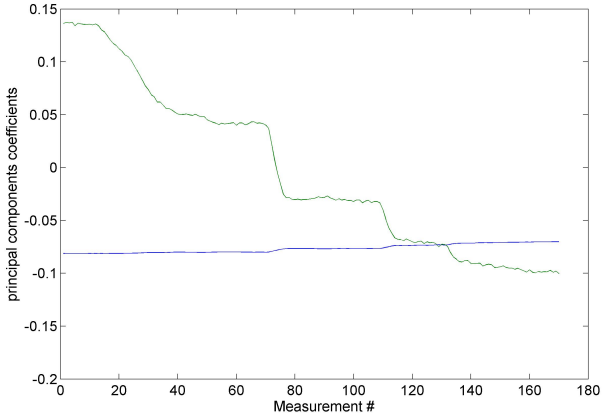

Figure 8.31: Behaviour of the 1^{st} and 2^{nd} Principal Components detected by SVD during a 5-step temperature transient.

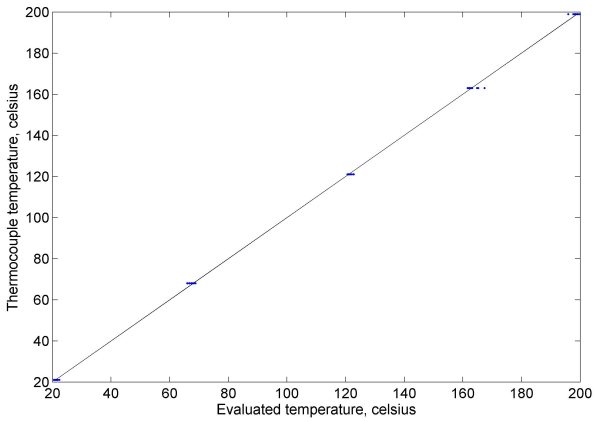

Figure 8.32: Linearity graph of the evaluated temperature, detected by linear calibration of the first two Principal Components referenced against thermocouple measurements, showing measurement reproducibility.

8.7.1 Method

The WMS system is constantly monitoring the intensity of each absorption line from the demodulated signal shown in figure 8.29. The resulting amplitudes measured during a 5-step temperature transient experiment is shown in figure 8.30. To avoid the additional complexity of a model for line ratios as a function of temperature, a multivariate analysis calibration approach was used.

Singular Value Decomposition was used on the matrix containing measured absorption intensities of 10 lines taken at different known temperatures, leading to identification of the principal components that can be linearly combined to give every possible line-amplitude profile in a temperature changing environment.

Figure 8.31 shows the behaviour of the first two principal components identified by the SVD algorithm running on the data set from the 5-step temperature transient.

The correct combination of the first (strongest) components found, the number of which depends on how extended is the measurement temperature range (two were enough for a +20 to +200 celsius range), is then found by inversion to obtain the known reference temperature. Using a matrix representation for the component values and considering the first 2 components, the calibration opera-

tion (which is done on k measurements provided with a reference measurement) leads to inversion of the following relation:

$$\begin{bmatrix} a_{11} & a_{12} \\ a_{21} & a_{22} \\ \vdots & \vdots \\ a_{k1} & a_{k2} \end{bmatrix} \begin{bmatrix} c_1 \\ c_2 \end{bmatrix} = \begin{bmatrix} T_1 \\ T_2 \\ \vdots \\ T_k \end{bmatrix}$$

where a_{ij} is the j-th principal component of the i-th calibration measurement, c_1 and c_2 are the two calibration coefficients to be resolved, T_i is the i-th temperature measurement provided by "expert answer" (thermocouple measurement).

Running this method on the 5-step temperature transient data set (after removal of data chunks corresponding to changing temperature intervals) gives the linearity graph from figure 8.32.

When performing an actual measurement the line peak amplitudes are first decomposed along the basis of principal components, then the coefficients of the first two components are linearly combined with calibration coefficients c_1 and c_2 to give T.

Chapter 9

Conclusions

The research presented in this work led to the developement of instrument prototypes which are ready for the next step of becoming products for the industrial market.

- The bottle gas analyzer is currently being integrated with the previously available carbon dioxide sensing setup to provide a single instrument for detection of both total pressure, oxygen concentration and carbon dioxide concentration; after this stage, testing on samples will determine actual oxygen concentration range commonly found in bottles, telling the real usefulness of the device;

- Double glazing glass oxygen measurement prototype is now ready for an extended testing on the field. While the current version of the instrument is capable of both static and dynamic concentration measurements, feedback from the industrial world could drive the final product design towards one or the other type of measurement. Testing on the field will also give feedback on topics such as determining the most suitable operating sequence, calibration requirements, interfacing with the gas filling equipment, operational temperature range, occurrence of different glass types; if required, improvements will be introduced to achieve a safe instrument functionality even in harsh industrial environments.

- The instrument for measurement on food packages with scattering surfaces will be proposed on the market and, being a sort of LIDAR, could even

be specialized for custom measurement ranges if required;

- GASMAS TDLAS WMS has been shown as a versatile laboratory technique to researchers in the food engineering field;
- The combined oxygen and water vapour fiber coupled GASMAS instrument from Lunds Universitet will lead to devices for use on fully scattering food packages and for medical diagnosis; before becoming an useful diagnostic tool, however, extensive testing and building of a clinical database will be required;
- Temperature measurement through oxygen TDLAS-WMS has been shown during workshops to researchers in the steelmaking industry, which is an already sensitive community about contact-free oxygen metering.

Bibliography

[1] T. Svensson et al., VCSEL-based oxygen spectroscopy for structural analysis of pharmaceutical solids, Appl. Phys. B 90, 345-354 (2008)

[2] Christopher R. Webster, Measuring methane and its isotopes $^{12}CH_4$, $^{13}CH_4$, and CH_3D on the surface of Mars with in situ laser spectroscopy, Applied Optics Vol. 44, No. 7, 1 March 2005

[3] S. Svanberg, Laser based diagnostics - from cultural heritage to human health, Appl. Phys. B (2008)

[4] U. Tylewicz, P. Lundin, L. Cocola, K. Dymek, P. Rocculi, S. Svanberg, P. Dejmek, F. G. Galindo, Gas in Scattering Media Absorption Spectroscopy (GASMAS) Detected Persistent Vacuum in Apple Tissue After Vacuum Impregnation, Food Biophysics, DOI: 10.1007/s11483-011-9239-7 (2011)

[5] L. R. Brown, C. Plymate, Experimental Line Parameters of the Oxygen A Band at 760 nm, Journal of Molecular Spectroscopy 199, 166-179 (2000)

[6] P. Lundin, L. Cocola, M. Lewander, A. Olsson, S. Svanberg, Non-intrusive headspace gas measurement by laser spectroscopy - performance validation by a reference sensor, submitted to J. Food Eng. (2011)

[7] L. Cocola, M. Fedel, I. Sirena, G. Tondello, Spettroscopia Ad Assorbimento Per La Misurazione Di CO2: Realizzazione di un afrometro Elettronico, La Chimica e l'Industria, ISSN: 0009-4315 (2010)

[8] L. Cocola, M. Fedel, G. Tondello, A New Device for the Measurement of Gaseous Oxygen in Closed Containers, Proceedings, The 3rd International Multi-Conference on Engineering and Technological Innovation, Orlando, Florida, USA, 1 luglio 2010, vol. 2, p. 79-81, ISBN: 978-1-936338-03-0 (2010)

[9] L. Cocola, M. Fedel, G. Tondello, Apparecchiatura per la misura della concentrazione di un gas in un contenitore chiuso, Brevetto PD2010A000203 (2010)